p53 Dynamics Control Cell Fate

Jeremy E. Purvis *et al.*

Science **336**, 1440 (2012);
DOI: 10.1126/science.1218351

Science (print ISSN 0036-8075; online ISSN 1095-9203) is published weekly, except the last week in December, by the American Association for the Advancement of Science, 1200 New York Avenue NW, Washington, DC 20005.

maximum uncertainty (Fig. 1 and fig. S1). For example, increased breakdown rates in slightly enriched streams would indicate altered ecosystem functioning, although most managers would consider such streams ecologically intact on the basis of traditional assessment criteria. Conversely, low breakdown rates at moderately enriched sites are no guarantee that streams are unaffected, requiring comprehensive assessments based on a range of indicators in order to draw conclusions about ecosystem impairment.

Our results raise fundamental questions about how to determine ecosystem health. First, naturally low-nutrient conditions are the desired state that water resource managers aspire to, and yet breakdown rates in such systems were indistinguishable from those in heavily polluted streams. This suggests that ensuring both low-nutrient water and effective resource use in stream food webs (from leaf litter to detritivores to fish) coupled with high process rates might be irreconcilable goals in stream management. Second, stream managers currently rely primarily on structural measures to assess stream ecosystem health. In particular, changes in biological community structure (invertebrates, fish, and algae) have long underpinned stream bioassessment schemes because they provide a reliable time-integrated response to stressors such as organic pollution or acidification (*5*), but biogeographical constraints make this approach difficult to standardize at large scales (*10*). Litter breakdown can help here because biogeography is a minor issue (for example, black alder or similar species of the genus are common throughout most of Europe and the Holarctic), and marked changes in breakdown rate occurred in the rising portion of the pollution gradient, in which established structural measures (such as water chemistry, hydromorphology, and metrics based on fish, invertebrate, or algal communities) are typically least sensitive. Consequently, litter breakdown—and potentially other functional measures such as whole-ecosystem metabolism, nutrient spiraling, or primary production (*26*–*28*)—can be used to complement, not replace, established procedures to assess stream ecosystem health. This highlights the need for differential diagnoses in environmental assessment, as is standard practice in medicine. Importantly, litter breakdown and some other functionally based methods can be implemented at relatively little cost or resource input (*29*) in order to assess effects of pollution and other ecosystem impacts that are of concern to environmental managers and stakeholders.

Increasing human pressure is accelerating environmental change throughout the world, threatening water security for humans and aquatic biodiversity (*2*). Large stretches of the landscape in Europe and other parts of the world are characterized today by highly industrialized, intensively managed agriculture and the large-scale application of fertilizers. This, in combination with other nutrient sources such as atmospheric deposition, has resulted in widespread nutrient pollution of aquatic ecosystems (*2*, *5*, *8*). Our study reveals that along with biodiversity losses, as fresh waters drift away from their natural conditions, ecosystem processes are profoundly changed, too. Impacts on stream functioning may go beyond the effects on litter breakdown because changing litter dynamics can have strong effects on nutrient retention and transformations (*27*), invertebrate productivity (*12*, *30*), and other functional ecosystem attributes. Given these complexities and large uncertainties surrounding human environmental impacts (*5*, *24*), a critical objective for the future will be to improve concepts and implementation tools to simultaneously manage surface waters sustainably and meet the demands of biodiversity conservation and environmental legislation.

References and Notes

1. A. M. Helton *et al.*, *Front. Ecol. Environ* **9**, 229 (2011).
2. C. J. Vörösmarty *et al.*, *Nature* **467**, 555 (2010).
3. E. S. Bernhardt *et al.*, *Science* **308**, 636 (2005).
4. P. H. Gleick, *Science* **302**, 1524 (2003).
5. N. Friberg *et al.*, *Adv. Ecol. Res* **44**, 2 (2011).
6. D. Hering *et al.*, *Sci. Total Environ.* **408**, 4007 (2010).
7. M. O. Gessner, E. Chauvet, *Ecol. Appl.* **12**, 498 (2002).
8. J. Hilton, M. O'Hare, M. J. Bowes, J. I. Jones, *Sci. Total Environ.* **365**, 66 (2006).
9. C. Perrings *et al.*, *Science* **330**, 323 (2010).
10. M. O. Gessner *et al.*, *Trends Ecol. Evol.* **25**, 372 (2010).
11. J. C. Moore *et al.*, *Ecol. Lett.* **7**, 584 (2004).
12. J. B. Wallace, S. L. Eggert, J. L. Meyer, J. R. Webster, *Science* **277**, 102 (1997).
13. J. L. Tank, E. J. Rosi-Marshall, N. A. Griffiths, S. A. Entrekin, M. L. Stephen, *J. N. Am. Benthol. Soc.* **29**, 118 (2010).
14. J. R. Webster, E. F. Benfield, *Annu. Rev. Ecol. Syst.* **17**, 567 (1986).
15. V. Gulis, K. Suberkropp, *Freshw. Biol.* **48**, 123 (2003).
16. A. D. Rosemond, C. M. Pringle, A. Ramírez, M. J. Paul, J. L. Meyer, *Limnol. Oceanogr.* **47**, 278 (2002).
17. C. F. Mason, *Biology of Freshwater Pollution* (Prentice-Hall, Upper Saddle River, NJ, ed. 4, 2002), p. 391.
18. M. Bundschuh, T. Hahn, M. O. Gessner, R. Schulz, *Environ. Toxicol. Chem.* **28**, 197 (2009).
19. M. Hieber, M. O. Gessner, *Ecology* **83**, 1026 (2002).
20. C. Pascoal, M. Pinho, F. Cassio, P. Gomes, *Freshw. Biol.* **48**, 2033 (2003).
21. Materials and methods are available as supplementary materials on *Science* Online.
22. C. J. F. ter Braak, P. Smilauer, *CANOCO Reference Manual and User's Guide to CANOCO for Windows: Software for Canonical Community Ordination* (Microcomputer Power, Ithaca, NY, 1998).
23. A. Lecerf *et al.*, *Arch. Hydrobiol.* **165**, 105 (2006).
24. L. Boyero *et al.*, *Ecol. Lett.* **14**, 289 (2011).
25. S. Hladyz *et al.*, *Adv. Ecol. Res* **44**, 211 (2011).
26. R. G. Young, K. J. Collier, *Freshw. Biol.* **54**, 2155 (2009).
27. P. J. Mulholland, J. R. Webster, *J. N. Am. Benthol. Soc.* **29**, 100 (2010).
28. P. J. Mulholland *et al.*, *Nature* **452**, 202 (2008).
29. M. J. Feio, T. Alves, M. Boavida, A. Medeiros, M. A. S. Graça, *Freshw. Biol.* **55**, 1050 (2010).
30. W. F. Cross, J. B. Wallace, A. D. Rosemond, S. L. Eggert, *Ecology* **87**, 1556 (2006).

Acknowledgments: We thank the European Commission and the Swiss State Secretariat for Research and Education for funding the RivFunction research project (European Union contract EVK1-CT-2001-00088), which was supported under the Fifth Framework Programme. The constructive comments by three anonymous reviewers, which substantially improved the paper, are greatly appreciated. All basic data are available in the supplementary materials. This paper is dedicated to the memory of our colleague Björn Malmqvist, who sadly passed away in 2010.

Supplementary Materials

www.sciencemag.org/cgi/content/full/336/6087/1438/DC1
Materials and Methods
Figs. S1 to S6
Table S1
Reference (*31*)
Databases S1 and S2

23 January 2012; accepted 26 April 2012
10.1126/science.1219534

p53 Dynamics Control Cell Fate

Jeremy E. Purvis, Kyle W. Karhohs, Caroline Mock, Eric Batchelor,* Alexander Loewer,† Galit Lahav‡

Cells transmit information through molecular signals that often show complex dynamical patterns. The dynamic behavior of the tumor suppressor p53 varies depending on the stimulus; in response to double-strand DNA breaks, it shows a series of repeated pulses. Using a computational model, we identified a sequence of precisely timed drug additions that alter p53 pulses to instead produce a sustained p53 response. This leads to the expression of a different set of downstream genes and also alters cell fate: Cells that experience p53 pulses recover from DNA damage, whereas cells exposed to sustained p53 signaling frequently undergo senescence. Our results show that protein dynamics can be an important part of a signal, directly influencing cellular fate decisions.

Cells use molecular signaling networks to sense, interpret, and respond to stimuli. Recent advances in time-lapse microscopy have revealed that many signaling molecules show complex dynamical behaviors (*1*–*13*). In some instances, dynamical properties such as oscillation frequency or signal duration, have been shown to alter gene expression (*1*, *3*, *6*, *8*, *11*, *13*–*16*) or to control cellular differentiation (*7*, *12*, *17*). These examples point to a rich mode of regula-

tion that is largely unexplored for most biological pathways. We developed a mathematically designed perturbation of p53 dynamics in response to DNA damage and have shown experimentally that p53 dynamics determine cellular responses.

p53 is a tumor suppressor activated in response to cellular stress (*18*, *19*). Induction of p53 triggers multiple cellular programs ranging from transient responses, such as DNA repair and cell cycle arrest, to terminal fates such as cell death (apoptosis) and permanent cell cycle arrest (senescence) (Fig. 1A). Recently, it was shown that different stresses evoke different dynamic patterns of p53 protein levels (Fig. 1B) (*20*). In response to DNA breaks caused by γ-irradiation, the levels of p53 exhibit a series of pulses with fixed amplitude and frequency (*4*, *21*). Higher radiation doses increase the number of pulses without affecting their amplitude or duration. These p53 pulses were observed in a live mouse model (*22*) and in various transformed and non-transformed human cell lines (*23*–*25*). In contrast, ultraviolet (UV) radiation triggers a single p53 pulse with a dose-dependent amplitude and duration (*20*). Although much insight has been gained into the molecular mechanisms that control these differential p53 dynamics in response to γ and UV radiation (*20*, *25*, *26*), the effect of p53 dynamics on downstream responses remains unknown. UV and γ radiation activate distinct targets of p53 (*27*) and lead to different cellular outcomes (Fig. 1B), suggesting that downstream elements in the p53 network may respond to the dynamic profiles of p53. However, γ and UV radiation also lead to many p53-independent events in cells, which could contribute to the differential outcomes. A definitive conclusion about the role of p53 dynamics on cellular outcomes may come from experimentally perturbing p53 dynamics in response to the same stress and observing the effect on downstream responses.

We developed a method for altering p53 dynamics after γ-irradiation. Our goal was to switch p53 natural pulses into a sustained p53 signal held at the peak pulse amplitude (Fig. 1C). We used the small molecule Nutlin-3, which binds to the p53 inhibitor Mdm2, inhibiting degradation of the p53 protein (*28*). Nutlin-3 is selective for p53 because $p53^{-/-}$ cells show no change in genome-wide expression profiling upon Nutlin-3 treatment (*29*). Achieving a sustained signaling response with a single Nutlin-3 treatment proved to be difficult: *MDM2* is activated by p53, and therefore, addition of Nutlin-3 not only stabilizes p53 but also causes an increase in Mdm2 levels that eventually overcomes Nutlin-3 inhibition, resulting in down-regulation of p53 (fig. S1). Treatment with a higher dose of Nutlin-3 led to prolonged induction of p53 but also to an overshoot in p53 levels (fig. S1). To overcome this obstacle, we trained our model of p53 dynamics (*26*) to predict the optimal sequence of Nutlin-3 additions necessary to sustain p53 at a constant level (Fig. 1D, fig. S2, and tables S1 and S2). The model predicted that three sequential treatments of Nutlin-3 at 2.5 hours (0.75 μM), 3.5 hours (2.25 μM), and 5.5 hours (4 μM) after γ-irradiation would produce a sustained p53 response with an amplitude equal to p53 natural pulses. This prediction was validated experimentally in both cell populations and single cells (Fig. 1E and fig. S3). These two dynamical "inputs"—naturally pulsed and pharmacologically sustained p53 signaling (hereafter, "pulsed" and "sustained")—were then used to study the downstream effects of p53 dynamics on target gene expression and cellular outcome.

Department of Systems Biology, Harvard Medical School, Boston, MA 02115, USA.

*Present address: Laboratory of Pathology, National Cancer Institute, National Institutes of Health, Bethesda, MD 20892, USA.

†Present address: Berlin Institute for Medical Systems Biology, Max Delbrueck Center for Molecular Medicine, Berlin-Buch 13125, Germany.

‡To whom correspondence should be addressed. E-mail: galit@hms.harvard.edu

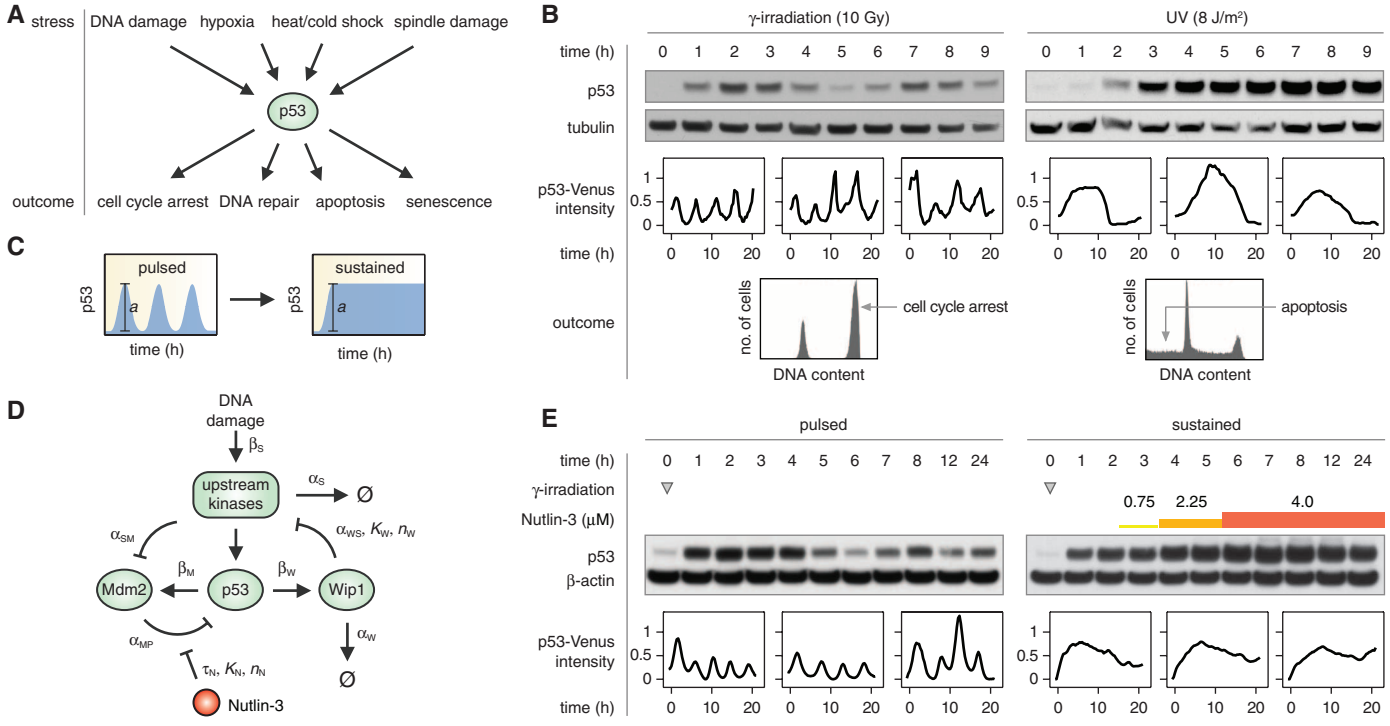

Fig. 1. Perturbation of p53 dynamics. (**A**) p53 mediates the response to multiple cellular stresses and evokes diverse cellular outcomes. (**B**) γ-irradiation leads to p53 pulses and cell cycle arrest; UV radiation induces a single prolonged pulse and leads to apoptosis. (**C**) p53's natural pulses were perturbed to produce a sustained response with equal amplitude, *a*. (**D**) A diagram capturing the main species and parameters in the mathematical model of p53 dynamics after DNA damage (*26*). This model was used to predict the optimal sequence of Nutlin-3 additions needed to generate a sustained p53 response after γ-irradiation (supplementary materials). (**E**) p53 dynamics under (left) naturally pulsed or (right) pharmacologically sustained conditions. The sequence of Nutlin-3 treatments is denoted by differently colored bars. Pulses in immunoblots appear as damped oscillations because of the asynchronous responses of single cells. Representative single-cell traces show average nuclear p53-Venus intensities that were normalized to the median value and zeroed to the minimum value. Sequential Nutlin-3 treatment did not alter the amplitude of p53 (fig. S3).

To understand how p53 dynamics control gene expression, we selected a panel of well-studied p53 target genes representing different functional pathways and cellular outcomes (*30*). A subset of genes showed a clear oscillatory response that mirrored p53 protein dynamics (Fig. 2, A and B, and table S3). This group included genes involved in cell cycle arrest and DNA repair (*CDKN1A*, *GADD45A*, and *XPC*), as well as genes known to regulate p53 levels (*MDM2* and *PPM1D*). In contrast, transcripts encoding apoptotic proteins (*APAF1*, *BAX*, and *TP53AIP*) or involved in p53-dependent senescence (*PML* and *YPEL3*) (*31*, *32*) were not induced by p53 pulses (Fig. 2, C and D).

We next measured expression of these transcripts using our dynamic drug treatment (Fig. 1E) to sustain p53 signaling. Oscillating genes (such as *MDM2* and *CDKN1A*) showed sustained increases in expression. Genes involved in apoptosis or senescence—which were not induced by p53 pulses—showed either no induction (*APAF1* and *TP53AIP1*) or a delayed increase in expression (*BAX*, *PML*, and *YPEL3*) under sustained p53 signaling. These trends were p53-dependent (fig. S4). Taken together, these results indicate that p53 pulses selectively activate genes involved in transient responses to DNA damage, whereas sustained p53 signaling allows induction of genes associated with terminal fates.

We next asked whether changes in p53 dynamics lead to different cell fates—specifically, whether sustained p53 will trigger irreversible fates such as apoptosis or senescence, whereas pulsed p53 will allow recovery and growth. DNA content analysis by means of flow cytometry revealed only a small amount of cell death under both pulsed and sustained p53 conditions (fig. S5). We therefore pursued the alternate possibility that sustained p53 signaling promotes cellular senescence, a state of permanent cell cycle arrest (*33*, *34*). Cells were subjected to pulsed or sustained p53 signaling at several γ-irradiation doses and then assayed for senescence-associated β-galactosidase (β-gal) activity and their ability to proliferate in fresh growth media (fig. S6). At lower doses of γ-irradiation [2.5 and 5 grays (Gy)], sustained p53 signaling led to large increases in β-gal–positive cells (Fig. 3, A and B). At these levels of DNA damage, the majority of cells exposed to pulsed p53 were able to undergo multiple rounds of growth and division after recovery (Fig. 3, C to E, and fig. S7), whereas sustained p53 signaling reduced this fraction substantially, leading to a characteristically flattened morphology and an apparent inability to divide (Fig. 3C). These differences were most pronounced after 5 Gy of γ-irradiation—a dose at which nearly all cells showed a permanent arrest after sustained p53 signaling (Fig. 3, D and E). Sustained p53 signaling at 2.5 Gy led to a greater fraction of senescent cells than did pulsed p53 at 5 Gy (Fig. 3, B and E), suggesting that it is not the extent of DNA damage that induces senescence, but rather the dynamics of p53 signaling.

We did not observe a large difference in β-gal activity or in proliferative ability at the highest dose of γ-irradiation (10 Gy). This suggested that prolonged p53 pulsing (*4*, *21*, *25*) caused by extensive DNA damage might eventually lead to expression of senescence genes. Indeed, we found that after 3 days under pulsed conditions, the p53-dependent senescence genes were induced to similar levels reached under sustained conditions after 1 day (Fig. 3F). *CDKN1A*, which is involved in both cell cycle arrest and p53-dependent senescence (*33*, *34*), showed the most dramatic increase in expression (>100-fold) under sustained p53 signaling.

Thus, sustained p53 signaling appears to accelerate the expression of senescence genes, whereas pulsed p53 delays gene expression and so protects cells from prematurely committing to an irreversible fate. However, by the time a cell commits to senescence the total amount of p53 accumulated over time ("cumulative p53") is

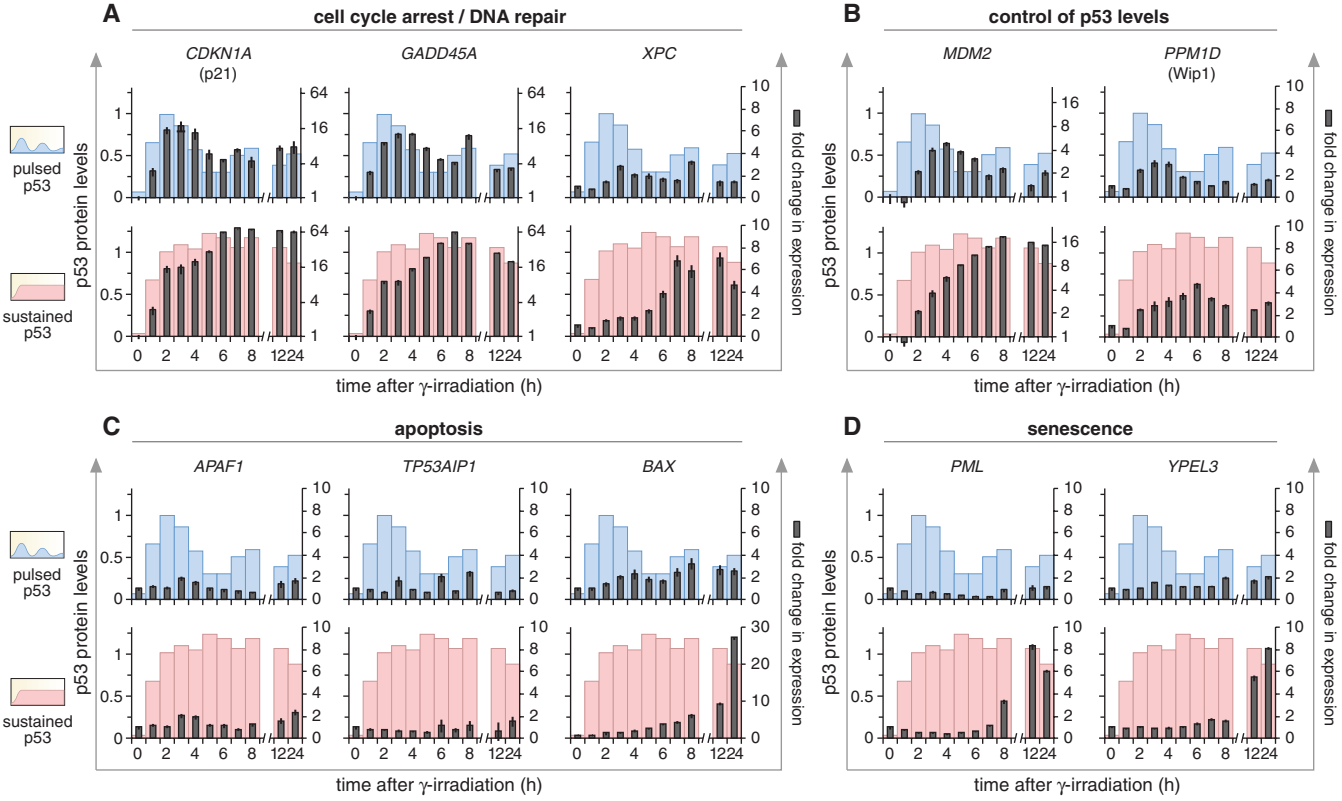

Fig. 2. Pulsed and sustained p53 signaling activate different sets of target genes. Expression of p53 target genes was measured under pulsed or sustained conditions after γ-irradiation. Genes are grouped according to function: (**A**) cell cycle arrest and DNA repair, (**B**) control of p53 levels, (**C**) apoptosis, and (**D**) senescence. For reference, p53 protein levels are shown in the background as light blue (pulsed) or red (sustained) bars. p53 levels are normalized to the peak (t = 2 hours) p53 concentration. A base-2 logarithmic scale is used for *CDKN1A*, *GADD45A*, and *MDM2*. Data are mean ± SD. Significance of correlation between target genes and p53 protein levels under pulsed conditions is reported in table S3.

much higher under sustained conditions than in pulsing cells. To determine whether this change in cell fate is due to p53 dynamics or merely to an increase in cumulative p53, we compared expression of senescence genes between pulsed and sustained p53 at equivalent levels of cumulative p53 (Fig. 4A). We found that even for similar cumulative p53, sustained p53 signaling led to higher expression of its target genes than pulsed p53, suggesting that it is the dynamics of p53 rather than its accumulated levels that control gene expression.

We further tested this in single cells. We first showed that individual senescent cells have significantly higher levels of *CDKN1A* and *PML* transcripts than those of proliferating cells (fig. S8), confirming that these transcripts are reliable markers for the induction of senescence. We then quantified p53 dynamics under pulsed and sustained conditions and used fluorescence in situ hybridization (FISH) to compare the level of *CDKN1A* and *PML* (Fig. 4, B and C). To achieve comparable cumulative p53 levels between pulsed and sustained p53, we terminated pulsed p53 21 hours after irradiation (t_1) and sustained p53 12 hours after irradiation (t_2) (Fig. 4D). We found that expression of both *CDKN1A* and *PML* was significantly higher under sustained p53 than under pulsed p53 even at similar cumulative p53 levels (Fig. 4, E and F). These results suggest that the decision of whether and when to enter senescence is communicated to cells through the temporal pattern of p53 (Fig. 4G).

It is well established that different posttranslational modifications of p53 or different cofactors that bind p53 affect the choice of downstream gene programs (*35*). Here, we have shown another mechanism for specificity in this network: the dynamics of p53. Our work suggests that p53 dynamics are important but do not act alone: p53 signaling produced by γ-irradiation and Nutlin-3 leads to senescence, whereas a comparable dynamical profile in response to UV radiation leads to apoptosis (Fig. 1B). Future studies are required to explore the combined effect of p53 dynamics and modifications on cellular outcomes.

What molecular mechanism may decode p53 dynamics to determine cell fate? One hypothesis is that p53 pulses periodically exceed a threshold concentration for transcriptional activation of senescence genes. In this scenario, sustained p53 or a greater number of p53 pulses increases the probability that p53 will activate downstream targets that are involved in the induction of senescence. A similar mechanism was previously reported (*14*), in which the frequency of calcium oscillations controls specificity for activation of proinflammatory transcription factors. Another plausible mechanism involves a feed-forward loop motif that discriminates transient and persistent p53 signaling. This type of mechanism was identified in the extracellular signal-related kinase (ERK) signaling pathway, in which the early gene product c-Fos functions as a sensor for sustained ERK levels (*17*). By analogy, an early gene induced by p53 and essential for activating senescence with p53 may decay with a time scale close to the time scale of p53 pulses and therefore accumulates slowly during p53 pulses, but more rapidly during a sustained p53 response. It is also possible that expression of senescence genes is initially repressed, for example, by epigenetic silencing or antisense RNA, and that these factors are deactivated by persistent p53 signaling.

Other signaling pathways have been shown to encode information through the dynamics of their signaling molecules (*1–3*, *5–13*), suggesting that varying protein dynamics may offer a functional advantage in certain contexts. For example, information encoded in the dynamics, rather than the absolute concentration of a signaling molecule, may be less sensitive to spontaneous fluctuations in the cellular environment. In addition, certain dynamical patterns may allow neighboring cells to synchronize their responses to produce emergent multicellular behaviors. A better understanding of how signaling dynamics are regulated and how they affect cellular responses will provide new insights for manipulating them in a controlled way. In addition, targeted perturbation of protein dynamics, such as the one illustrated in this study, may enable new pharmacological strategies for altering cell fate in a range of diseases.

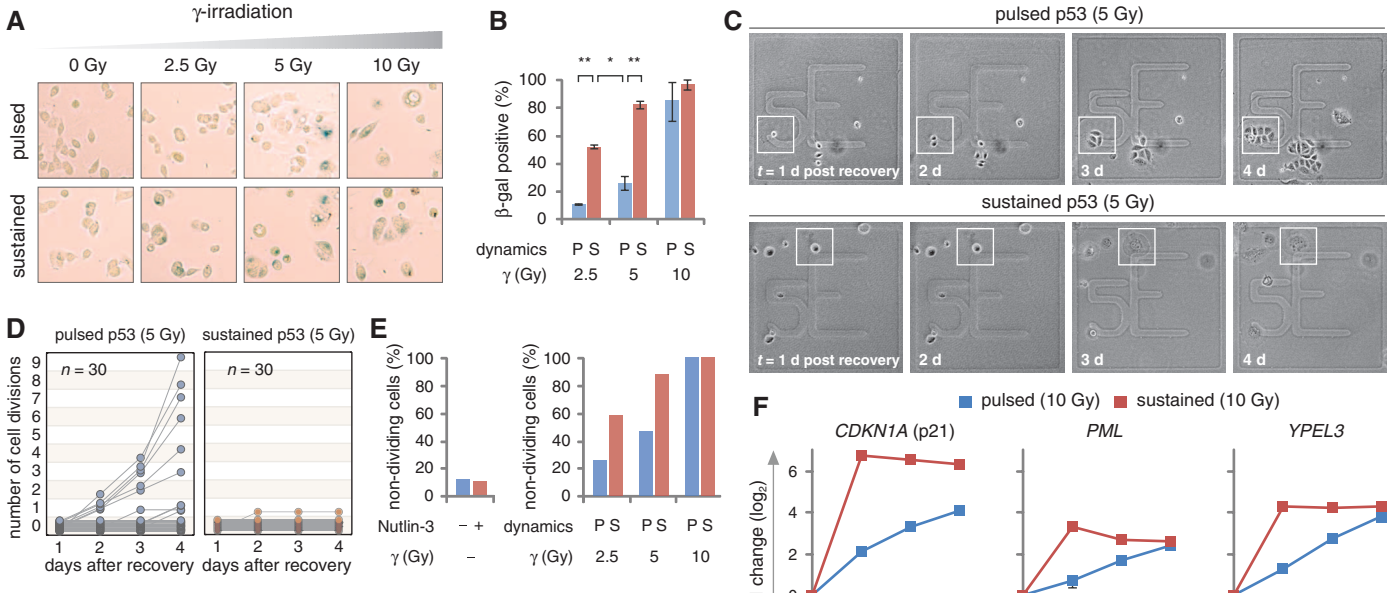

Fig. 3. Pulsed and sustained p53 signaling lead to different cell fates. (**A**) Cells were subjected to pulsed (top) or sustained (bottom) conditions for 3 days and then stained for β-gal activity 1 day after recovery. Blue color and flattened morphology are indicative of senescence. (**B**) Percentage of β-gal-positive cells under pulsed (P) or sustained (S) p53 signaling at various γ-irradiation doses. $n \geq 100$ cells per condition per experiment. *$P < 0.05$, **$P < 0.01$. (**C**) Typical images of single cells that were recovered after 3 days of pulsed (top) or sustained (bottom) p53 signaling at 5 Gy γ-irradiation. White boxes are drawn to show the fate of an individual cell. (**D**) Number of cell divisions for single cells after recovery from pulsed or sustained p53 signaling at 5 Gy. (**E**) (Left) Percentage of cells that did not divide under resting conditions or sequential Nutlin-3 treatment alone (no γ-irradiation). (Right) Percentage of nondividing cells under pulsed (P) or sustained (S) p53 signaling. (**F**) Fold change in expression of *CDKN1A*, *PML*, and *YPEL3* after 24, 48, and 72 hours under pulsed (blue) or sustained (red) p53 signaling (10 Gy γ-irradiation). Expression levels were normalized to *ACTB*. Data are mean ± SD.

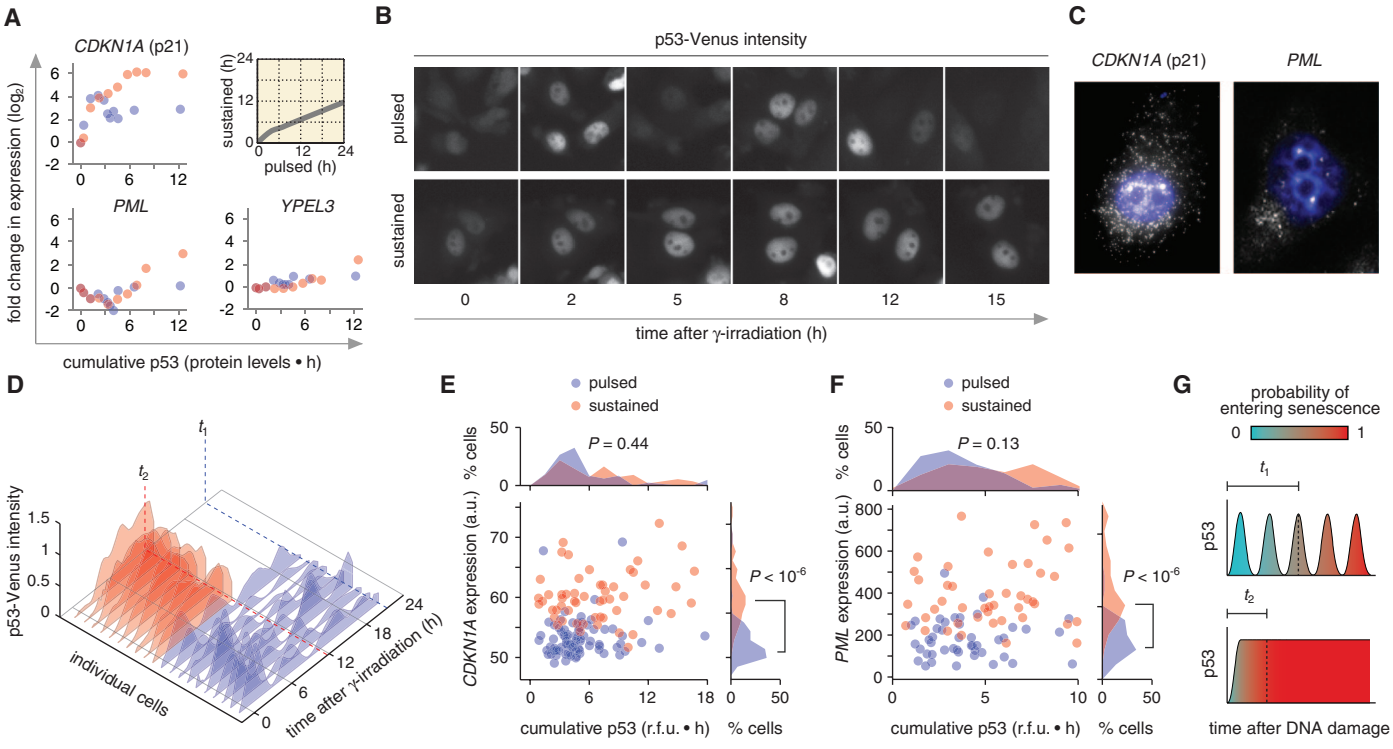

Fig. 4. p53 dynamics, and not its cumulative level, control cell fate. (**A**) (Inset) Time points for which pulsed and sustained p53 signaling show equivalent cumulative p53 levels [$\int p53(t)dt$] lie along the gray line. Gene expression under pulsed (blue dots) or sustained (red dots) p53 signaling are plotted as a function of cumulative p53 by using the data presented in Fig. 1E. The time integral of p53 protein levels was computed by using trapezoidal integration of p53 levels over time. Gene expression was normalized to *ACTB*. The last time point in sustained conditions (24 hours) was omitted because there is no comparable data point under pulsed conditions. (**B**) p53 dynamics were recorded by means of live-cell microscopy under pulsed and sustained conditions. (**C** and **D**) Representative single-cell traces of p53 levels under (blue) pulsed or (red) sustained conditions. Time-lapse imaging was terminated by fixing cells 21 hours after irradiation (pulsed conditions, t_1) or 12 hours after irradiation (sustained conditions, t_2) and probing for expression of *CDKN1A* or *PML* by means of FISH. (**E**) *CDKN1A* and (**F**) *PML* expression versus cumulative p53 in individual cells. a.u., arbitrary units; r.f.u., relative fluorescence units (supplementary materials). (**G**) Model for p53 dynamics controlling cell fate. Transient damage encountered under low-radiation dose or physiological conditions is repaired quickly and generates a small number of p53 pulses, allowing the cell to continue dividing. Persistent damage—whether from a large number of initial DNA lesions or a small number of irreparable breaks—generates repeated p53 pulses that ultimately trigger cellular senescence. t_1 and t_2 represent time points in which the cumulative level of p53 is equal between pulsed and sustained conditions. However, the probability of entering senescence differs between these two types of dynamics. Pulsed p53 allows more time for recovery from DNA damage, whereas sustained p53 accelerates this process.

References and Notes

1. L. Cai, C. K. Dalal, M. B. Elowitz, *Nature* **455**, 485 (2008).
2. N. Hao *et al.*, *Mol. Cell* **30**, 649 (2008).
3. A. Hoffmann, A. Levchenko, M. L. Scott, D. Baltimore, *Science* **298**, 1241 (2002).
4. G. Lahav *et al.*, *Nat. Genet.* **36**, 147 (2004).
5. J. T. Mettetal, D. Muzzey, C. Gómez-Uribe, A. van Oudenaarden, *Science* **319**, 482 (2008).
6. D. E. Nelson *et al.*, *Science* **306**, 704 (2004).
7. G. M. Süel, J. Garcia-Ojalvo, L. M. Liberman, M. B. Elowitz, *Nature* **440**, 545 (2006).
8. S. Tay *et al.*, *Nature* **466**, 267 (2010).
9. J. J. Ventura *et al.*, *Mol. Cell* **21**, 701 (2006).
10. T. K. Lee *et al.*, *Sci. Signal.* **2**, ra65 (2009).
11. S. L. Werner, D. Barken, A. Hoffmann, *Science* **309**, 1857 (2005).
12. S. D. Santos, P. J. Verveer, P. I. Bastiaens, *Nat. Cell Biol.* **9**, 324 (2007).
13. L. Ashall *et al.*, *Science* **324**, 242 (2009).
14. R. E. Dolmetsch, K. Xu, R. S. Lewis, *Nature* **392**, 933 (1998).
15. M. H. Sung *et al.*, *PLoS ONE* **4**, e7163 (2009).
16. N. Hao, E. K. O'Shea, *Nat. Struct. Mol. Biol.* **19**, 31 (2012).
17. L. O. Murphy, S. Smith, R. H. Chen, D. C. Fingar, J. Blenis, *Nat. Cell Biol.* **4**, 556 (2002).
18. H. F. Horn, K. H. Vousden, *Oncogene* **26**, 1306 (2007).
19. B. Vogelstein, D. Lane, A. J. Levine, *Nature* **408**, 307 (2000).
20. E. Batchelor, A. Loewer, C. Mock, G. Lahav, *Mol. Syst. Biol.* **7**, 488 (2011).
21. N. Geva-Zatorsky *et al.*, *Mol. Syst. Biol.* **2**, 2006, 0033 (2006).
22. D. A. Hamstra *et al.*, *Cancer Res.* **66**, 7482 (2006).
23. W. Hu *et al.*, *Cancer Res.* **67**, 2757 (2007).
24. R. Lev Bar-Or *et al.*, *Proc. Natl. Acad. Sci. U.S.A.* **97**, 11250 (2000).
25. A. Loewer, E. Batchelor, G. Gaglia, G. Lahav, *Cell* **142**, 89 (2010).
26. E. Batchelor, C. S. Mock, I. Bhan, A. Loewer, G. Lahav, *Mol. Cell* **30**, 277 (2008).
27. R. Zhao *et al.*, *Genes Dev.* **14**, 981 (2000).
28. L. T. Vassilev *et al.*, *Science* **303**, 844 (2004).
29. C. Tovar *et al.*, *Proc. Natl. Acad. Sci. U.S.A.* **103**, 1888 (2006).
30. T. Riley, E. Sontag, P. Chen, A. Levine, *Nat. Rev. Mol. Cell Biol.* **9**, 402 (2008).
31. E. de Stanchina *et al.*, *Mol. Cell* **13**, 523 (2004).
32. K. D. Kelley *et al.*, *Cancer Res.* **70**, 3566 (2010).
33. J. Campisi, F. d'Adda di Fagagna, *Nat. Rev. Mol. Cell Biol.* **8**, 729 (2007).
34. F. d'Adda di Fagagna, *Nat. Rev. Cancer* **8**, 512 (2008).
35. A. M. Bode, Z. Dong, *Nat. Rev. Cancer* **4**, 793 (2004).

Acknowledgments: We thank R. Agami for the MCF7/p53shRNA cell line; B. Fang for the MCF7/Casp3 cell line; A. Raj and Z. Waks for help with mRNA FISH; R. Kishony, R. Ward, W. Forrester, E. O'Shea, T. Mitchison, A. Klein, J. Orth, and U. Alon for comments and discussions; and the Nikon Imaging Center at Harvard Medical School for help with light microscopy. This research was supported by the Novartis Institutes for Biomedical Research, the National Institutes of Health grant GM083303 and fellowship F32GM095168 (J.E.P), a National Science Foundation graduate fellowship (K.W.K), the American Cancer Society, California Division, Pamela and Edward Taft Postdoctoral Fellowship (E.B.), and fellowships from the German Research Foundation and the Charles A. King Trust (A.L.). J.E.P and G.L. conceived the study, designed the experiments, and wrote the paper. J.E.P modeled and designed perturbation experiments and performed gene expression and cell fate assays, live-cell microscopy, single-cell mRNA detection, and image analysis. K.W.K. performed live-cell microscopy, single-cell mRNA detection, and image analysis. C.M. characterized p53 and p53-Venus dynamics under radiation and various drug treatments. E.B. and A.L. performed UV treatment experiments and provided preliminary results and foundational concepts.

Supplementary Materials

www.sciencemag.org/cgi/content/full/336/6087/1440/DC1
Materials and Methods
Figs. S1 to S8
Tables S1 to S5
References (*36*, *37*)

22 December 2011; accepted 1 May 2012
10.1126/science.1218351

Cell

A Role for the Nucleoporin Nup170p in Chromatin Structure and Gene Silencing

David W. Van de Vosse,[1,6] Yakun Wan,[2,3,6] Diego L. Lapetina,[1] Wei-Ming Chen,[2,4] Jung-Hsien Chiang,[4] John D. Aitchison,[2,5,*] and Richard W. Wozniak[1,*]
[1]Department of Cell Biology, University of Alberta, Edmonton, Alberta T6G 2H7, Canada
[2]Institute for Systems Biology, Seattle, WA 98109, USA
[3]The Key Laboratory of Developmental Genes and Human Disease, Ministry of Education, Institute of Life Sciences, Southeast University, Nanjing 210096, China
[4]Department of Computer Science and Information Engineering, National Cheng Kung University, Tainan 701, Taiwan
[5]Seattle Biomedical Research Institute, Seattle, WA 98109, USA
[6]These authors contributed equally to this work
*Correspondence: john.aitchison@systemsbiology.org (J.D.A.), rick.wozniak@ualberta.ca (R.W.W.)
http://dx.doi.org/10.1016/j.cell.2013.01.049

SUMMARY

Embedded in the nuclear envelope, nuclear pore complexes (NPCs) not only regulate nuclear transport but also interface with transcriptionally active euchromatin, largely silenced heterochromatin, as well as the boundaries between these regions. It is unclear what functional role NPCs play in establishing or maintaining these distinct chromatin domains. We report that the yeast NPC protein Nup170p interacts with regions of the genome that contain ribosomal protein and subtelomeric genes, where it functions in nucleosome positioning and as a repressor of transcription. We show that the role of Nup170p in subtelomeric gene silencing is linked to its association with the RSC chromatin-remodeling complex and the silencing factor Sir4p, and that the binding of Nup170p and Sir4p to subtelomeric chromatin is cooperative and necessary for the association of telomeres with the nuclear envelope. Our results establish the NPC as an active participant in silencing and the formation of peripheral heterochromatin.

INTRODUCTION

The nuclear envelope (NE) functions as a barrier between the genome and the cytoplasm. To regulate the exchange of macromolecules between the cytoplasm and the nucleus, molecules must traverse large, proteinaceous channels, termed nuclear pore complexes (NPCs), that extend across the NE. The role of NPCs in nuclear transport has been extensively studied (reviewed in Aitchison and Rout, 2012). NPCs are cylindrical channels composed of repetitive subunits that are organized with 8-fold symmetry around the central axis. Thus, despite its considerable mass (~50 MDa in yeast), an NPC is composed of only ~30 proteins, termed nucleoporins or Nups, which are present in multiple copies (Rout et al., 2000). The NPC is composed of membrane proteins, a symmetrical core scaffold containing the Nup84p and Nup170p-Nup157p complexes, and FG-Nups that populate the central channel and form cytoplasmic fibrils and a nuclear basket structure. The FG-Nups interact with transport factors and directly facilitate nucleocytoplasmic transport.

The NPC and other features of the NE also provide attachment sites for the underlying chromatin, and each establishes a distinct environment for chromatin. For example, transcriptionally silenced heterochromatin preferentially associates with the inner nuclear membrane (INM) (reviewed in Taddei et al., 2010), whereas active genes appear to be associated with the NPC. In *Saccharomyces cerevisiae*, the silent mating type loci and telomeres are associated with the INM, and anchoring of chromatin at the INM promotes silencing (Andrulis et al., 1998). A contributing factor to this peripheral gene silencing is the local concentration of the silent information regulator (SIR) complex, comprising Sir2p, Sir3p, and Sir4p (Gotta et al., 1996; Gasser et al., 2004), at the NE. These proteins bind subtelomeric and telomeric chromatin, and along with the yKu70/yKu80 dimer mediate telomere binding to the INM proteins Mps3p and Esc1p (reviewed in Taddei et al., 2010).

NPCs have long been postulated to tether chromosomal loci at the NE. Morphological observations of metazoan cells have revealed euchromatin channels extending from NPCs into the nucleoplasm and penetrating peripheral heterochromatin, positioning NPCs at the interface between these two chromatin states. Recent analyses of NPC–chromatin interactions in yeast have identified NPCs in association with transcriptionally active chromatin, silenced chromatin, and boundary chromatin, which displays characteristics of both states. Multiple Nups have been detected in association with active genes, and certain genes exhibit Nup-dependent recruitment to the NE upon transcriptional activation (reviewed in Van de Vosse et al., 2011). Moreover, Nup2p has been shown to play a role in demarcating boundaries between active and silenced

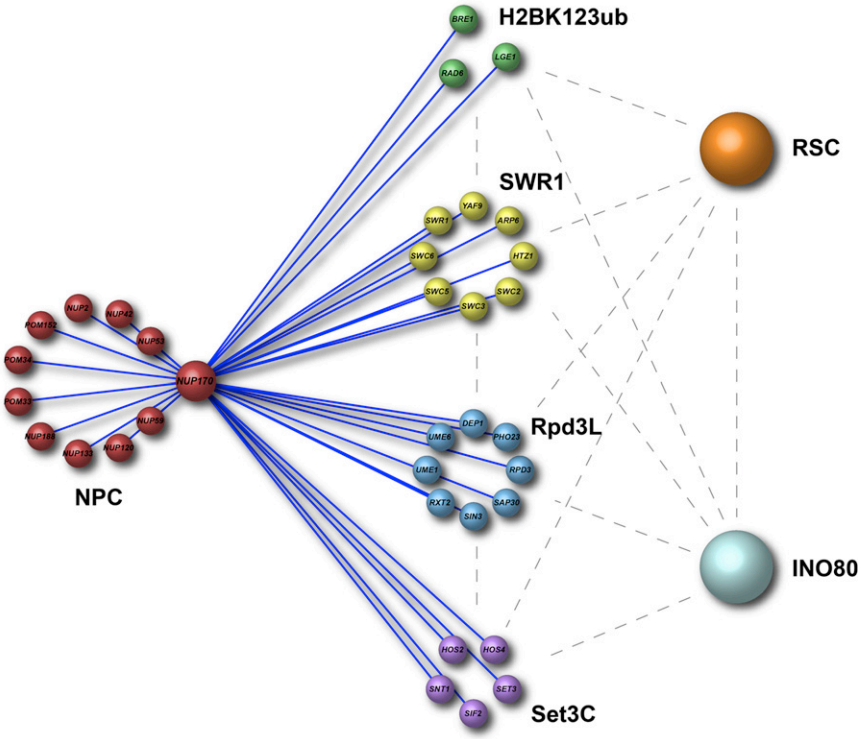

Figure 1. *NUP170* Functionally Interacts with Chromatin-Modifying Complexes

Cytoscape depicts genetic interactions between *NUP170* and genes encoding chromatin-modifying complexes. Nodes represent genes grouped by functional complexes. Edges connecting nodes represent synthetic genetic interactions. Only those interactions of *NUP170* with multiple components of a subcomplex are shown. Blue edges represent interactions identified by SGA analysis of *NUP170*, and gray dashed edges represent previously reported genetic interactions among chromatin complexes as denoted by the *Saccharomyces* Genome Database. See also Tables S1 and S2.

chromatin (Ishii et al., 2002; Dilworth et al., 2005). NPCs have also been proposed to organize silent chromatin domains at the NE, and two NPC-associated proteins, Mlp1p and Mlp2p, were implicated in telomere tethering at the NE (Galy et al., 2000; Feuerbach et al., 2002). However, these results were contested (Hediger et al., 2002a, 2002b). More recently, members of the Nup84 complex were implicated in both subtelomeric silencing and telomere tethering (Therizols et al., 2006).

How NPCs influence chromatin structure remains unknown, in large part due to a limited understanding of the molecular basis for their interactions. We investigated the role of a core component of the yeast NPC, Nup170p, in chromatin structure. Nup170p was implicated in the maintenance of heterochromatin structure in centromeric regions (Kerscher et al., 2001), and counterparts of Nup170p in higher eukaryotes are physically linked to chromatin-modifying complexes (Mendjan et al., 2006; Kehat et al., 2011). Here, we report physical and functional interactions between Nup170p and specific chromatin domains, including ribosomal protein (RP) genes and subtelomeric and telomeric regions. We show that Nup170p, through its interactions with the RSC chromatin-remodeling complex and the silencing factor Sir4p, is required for the formation of subtelomeric chromatin and its NE association.

RESULTS

Nup170p Functionally Interacts with Chromatin-Modifying Complexes

The combined functions of yeast Nup170p and its paralog, Nup157p, are essential for cell viability (Aitchison et al., 1995; Makio et al., 2009); however, strains lacking each protein are viable. Therefore, we used synthetic genetic array (SGA) analysis (Tong et al., 2001) to screen a nonessential gene deletion library for mutants that display epistatic interactions with null mutants of *NUP170* (*nup170Δ*). These interacting mutations are thought to compromise an essential structure or network, or two functionally redundant pathways that contribute to an essential cellular function. A total of 73 gene deletions displayed reduced fitness in combination with *nup170Δ*, predictably including NPC components (Figure 1; Table S1 available online). Notably, a significant proportion of the interacting genes (27 of 73; $p = 1.99 \times 10^{-15}$) encode subunits of complexes that function in chromatin organization, including chromatin remodeling (SWR1), histone deacetylation (Rpd3L and Set3C), and histone H2BK123 ubiquitination (Figure 1; Table S1). These interactions appeared to be specific for *NUP170*, since SGA analysis of *nup53Δ*, *nup60Δ*, or *kap123Δ* did not yield similar results (Table S1; Ptak et al., 2009) and the cohort of *NUP170* interacting genes did not show interactions with various other Nup genes (*NUP188*, *NUP157*, *NUP53*, or *NUP2*; Tables S1 and S2). Importantly, this role for Nup170p in chromatin organization is unlikely to be linked to nucleocytoplasmic transport, because the *nup170Δ* mutant has no detected defects in active transport (Aitchison et al., 1995; Makio et al., 2009), and its previously detected contribution to the NPC diffusion barrier is phenocopied by the *nup188Δ* mutant (Shulga et al., 2000), which did not display similar genetic interactions.

Nup170p Physically Interacts with the RSC Complex

We investigated the physical basis for the genetic interactions between mutations in *NUP170* and the chromatin-modifying complexes. Nup170-protein A (pA) was purified from strains producing GFP-tagged versions of representative members of the genetically interacting complexes. As expected, the Nup170p binding partner Nup53p was detected (Figure 2A; Lusk et al., 2002). However, with the exception of low levels of Rpd3-GFP, none of the GFP-tagged proteins were bound to Nup170-pA. These results implied a role for Nup170p in

a functionally overlapping pathway. Such a pathway is predicted to exhibit genetic interactions similar to those observed for the *nup170Δ* mutant. An analysis of databases revealed two chromatin-remodeling complexes, INO80 and RSC, that showed similar genetic interactions with the SWR1, Rpd3L, and Set3C complexes (Figure 1 and BioGRID; Stark et al., 2006). An examination of Nup170-pA-bound proteins revealed Sth1p, the ATPase subunit of the RSC complex, but not INO80 subunits (Figure 2). By contrast, Sth1p was not detected bound to Nup84-pA or Nup188-pA. Reciprocal experiments using Sth1-pA also detected an association with Nup170p and Nup53p, as well as RSC complex members. Notably, Nup53p binding to Sth1-pA was dependent on Nup170p. We conclude that Nup170p physically associates with the RSC complex, potentially through its binding to Sth1p.

Nup170p Is Required for Silencing of Subtelomeric Genes

RSC catalyzes nucleosome restructuring events that play a role in DNA double-strand break repair, telomere structure, and gene expression (Angus-Hill et al., 2001; Askree et al., 2004; Shim et al., 2005). To begin to assess the role of Nup170p in these functions, we examined the cellular transcription profile of the *nup170Δ* mutant using DNA microarrays. This analysis revealed 424 open reading frames (ORFs) upregulated and 59 ORFs downregulated >2-fold in the *nup170Δ* mutant. Strikingly, the upregulated genes were enriched for RP genes (109 of 138 RP genes, $p = 1.85 \times 10^{-105}$; p values by one-tailed Fisher's exact test) and genes positioned in subtelomeric regions (i.e., within 25 kb of telomeres). The smaller number of downregulated ORFs was randomly distributed throughout the genome (Figure 3A). Although they housed only ~6% of all ORFs, the subtelomeric regions contained ~28% of the genes upregulated in *nup170Δ* cells (119 of 424, $p = 1.94 \times 10^{-56}$), and ~34% of subtelomeric ORFs (119 of 347) showed alleviated repression (see Table S3). By contrast, gene-expression changes in *nup157Δ* and *nup188Δ* cells showed no enrichment of subtelomeric regions (Figure 3A).

DNA microarray analysis was also performed on cells depleted of Sth1p. *STH1* is an essential gene. Thus, to regulate its expression, the *STH1* promoter was replaced with the *MET3* promoter (P_{MET3}-*STH1*), allowing rapid depletion of Sth1p to barely detectable levels 4 hr after methionine repression (Figure 3B). We interrogated the transcriptome of P_{MET3}-*STH1* cells 2 hr after repression, at which point *STH1* messenger RNA (mRNA) levels were reduced ~4.4-fold and Sth1p levels were down ~2-fold (data not shown). Similar to the case with *nup170Δ* cells, we observed a pattern of subtelomeric derepression (Figure 3C), which could be reversed by reinduction of *STH1*.

Our microarray data are consistent with a role for Nup170p and RSC in subtelomeric gene silencing. We evaluated this function further using cell growth assays that provide a readout for the transcriptional state of two reporter genes, *URA3* and *ADE2*, inserted into subtelomeric regions adjacent to telomeres VII-L (Tel7L) and V-R (Tel5R; Figure 3D). Repression of these genes prevents growth in the absence of uracil and adenine but allows cells to grow in the presence of 5-fluoroorotic acid (5-FOA), whereas loss of a silencing factor (e.g., Sir3p) favors derepression of *URA3* and *ADE2*, allowing cell growth on medium lacking adenine and uracil, but rendering them sensitive to 5-FOA. *nup170Δ* cells showed similar silencing defects, which were reversed by an exogenous copy of *NUP170*. No silencing defects were detected in a *nup188Δ* mutant.

Although certain subunits of the RSC complex are essential, others are not, which allowed us to test the effects of mutations in several RSC components (e.g., *rsc1Δ*, *rsc3Δ*, *rsc7Δ*, and *htl1Δ*) on silencing of the *URA3* and *ADE2* reporter genes. Loss of silencing was most evident and reproducibly detected in the *rsc3Δ* and *htl1Δ* null mutants (Figures 3D and S1), albeit to a lesser extent than in either *nup170Δ* or *sir3Δ*. The milder silencing phenotypes of these *rsc* mutants may be explained by the fact that they do not compromise the essential function of RSC.

Loss of Nup170p Alters Nucleosome Positioning in Subtelomeric Chromatin

RSC is an important contributor to nucleosome structure, including the organization of a nucleosome-free region (NFR) adjacent to transcriptional start sites (TSS; Hartley and Madhani, 2009). The interactions of Nup170p with RSC and its role in transcription led us to examine subtelomeric chromatin structure in the absence of Nup170p using genome-wide nucleosome mapping. Across the genome, wild-type (WT) cells have a canonical positioning of the −1 and +1 nucleosomes flanking the NFR, followed by periodic phasing of downstream nucleosomes (Figures 4 and S2; see Weiner et al., 2010). By contrast, *nup170Δ* cells had reduced occupancy of the +1 nucleosome and, to a lesser extent, the −1 nucleosome (Figure 4A). The reduction in −1 and +1 nucleosome occupancy was more prominent within subtelomeric regions (0–25 kb), whereas adjacent regions (25–50 kb) showed little difference from the WT control. As with the subtelomeric regions, nucleosome profiles were also altered at RP genes (Figure 4A). These data further pointed to a role for Nup170p in defining chromatin structure within subtelomeric regions and RP genes.

We also examined the effect of Sth1p depletion on nucleosome position following *STH1* repression (Figure 4). As in previous reports (Hartley and Madhani, 2009), our genome-wide analysis revealed shrinkage of the NFR and a reduced occupancy of the +1 and −1 nucleosomes following Sth1p depletion. Clustering of subtelomeric and RP genes revealed similar changes (Figure 4B; data not shown). Of the subtelomeric genes that contained a recognizable TSS, 47 of 149 ORFs exhibited altered +1 nucleosome structure. Significantly, 42 ORFs showed similar changes in the *nup170Δ* mutant ($p = 1.05 \times 10^{-3}$), consistent with a functional relationship between Nup170p and RSC.

Nup170p Is Enriched at RP Genes and Subtelomeric DNA

To understand how Nup170p contributes to transcriptional repression, we investigated the physical interactions of Nup170p with chromatin. We performed chromatin immunoprecipitation (ChIP) analysis on strains producing Nup170p tagged with 9xMyc, and analyzed Nup170p-associated DNA using DNA microarrays (ChIP-chip). Predominant among the bound

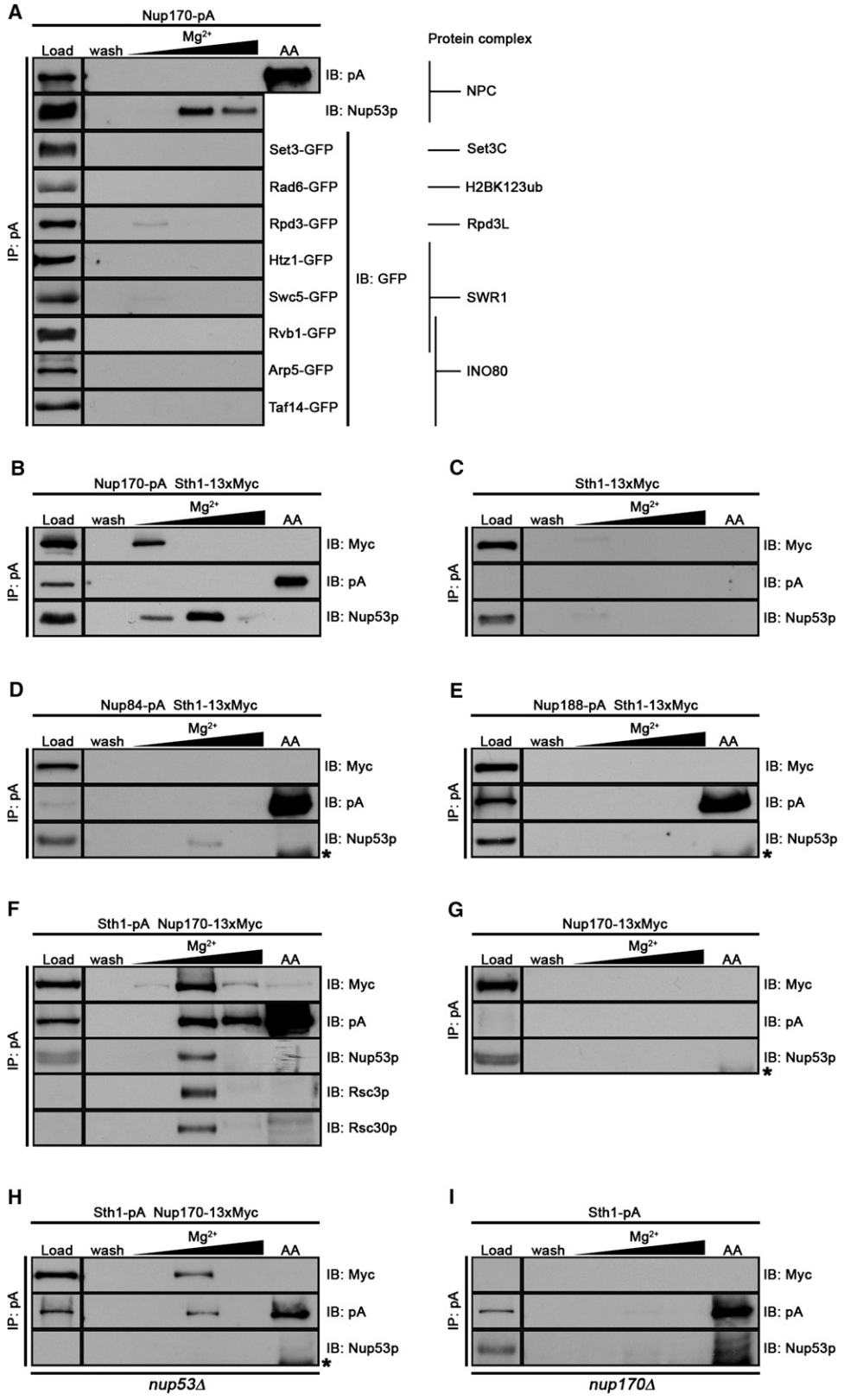

(legend on next page)

DNA fragments were regions adjacent to genes exhibiting increased expression in the absence of *NUP170*; of the 424 upregulated genes, 378 had probes on the microarray within 0.5 kb of the ORF, and 178 were detected in association with Nup170p ($p = 1.8 \times 10^{-49}$; Table S3). Prominent were regions of DNA near the chromosome ends (Nup170p-associated DNA bound 117 of 439 probes within 10 kb of telomeres; $p = 1.14 \times 10^{-48}$), corresponding to subtelomeric regions of 23 of 26 telomeres analyzed (Figures 5A, 5B, and S3). Here our ChIP-chip analysis detected a specific enrichment of Nup170p at many of the genes upregulated upon loss of Nup170p. Of the 119 genes within 25 kb of telomeres that exhibited increased expression upon deletion of *NUP170*, our microarrays contained probes for 75 within 0.5 kb of the ORF, and 57 of these were detected in association with Nup170p by ChIP-chip ($p = 8.1 \times 10^{-3}$; Tables S3 and S4). By contrast, ChIP-chip analysis did not reveal similar levels of Nup157p enrichment at specific sites within the genome. However, we observed modest binding to chromatin regions that showed the highest levels of Nup170p enrichment (see Figures 5 and S3), likely reflecting the physical association of Nup157p with Nup170p (Alber et al., 2007; Amlacher et al., 2011) and chromatin interactions mediated by Nup170p. These results were supported by real-time quantitative PCR (qPCR) assays that showed subtelomeric DNA adjacent to a representative telomere (Tel6R) was enriched with Nup170p but not with Nup157p or Nup188p (Figure 5D).

In addition to subtelomeric DNA, 131 of 138 RP genes were significantly enriched with Nup170p ($p = 3.3 \times 10^{-112}$; see Figure S4). These associations strongly correlated with the observed upregulation of 109 of 138 RP genes in the *nup170Δ* mutant (Figure S4). Thus, our results are consistent with Nup170p functioning as a transcriptional repressor that physically interacts with subtelomeric chromatin and RP genes.

Nup170p Association with Subtelomeric DNA Is Mediated by Sir4p

Transcriptional repression of subtelomeric genes has been extensively studied and various factors that contribute to this process have been identified. The yKu70/yKu80 heterodimer and the SIR complex are essential for subtelomeric chromatin structure and silencing. Since Nup170p lacks a detectable DNA-binding motif, we hypothesized that its role in silencing may be linked to these key silencing factors. Therefore, we examined whether Nup170p physically interacts with members of the yKu and SIR complexes. Analysis of Nup170-pA purified from cell extracts revealed Sir4-13xMyc, but not yKu70-13xMyc, bound to Nup170-pA (Figures 6A and 6B). Furthermore, we detected Nup170-13xMyc bound to purified Sir4-pA (Figure 6C). Since Sir4p binding to subtelomeric chromatin is mediated by the DNA-binding protein Rap1p, we also purified Rap1-pA. As with Sir4-pA, Nup170-13xMyc bound to Rap1-pA (Figure 6D). The specificity of the Sir4p–Nup170p interaction was also supported by experiments showing that Nup157p, a binding partner of Nup170p, bound to Sir4p, whereas Nup84p, a member of a distinct NPC subcomplex, did not (Figures 6E and 6F).

The association of Nup170p with Sir4p led us to examine whether Nup170p binding to subtelomeric chromatin required Sir4p. In the absence of Sir4p (*sir4Δ*), the enrichment of Nup170p at many of its subtelomeric chromatin-binding sites (most dramatically at 19 of 23 analyzed) was reduced, whereas its association with nonsubtelomeric DNA was largely unaffected (Figures 6H and S5). By contrast, the loss of yKu70p (*yKu70Δ*) did not affect the DNA-binding profile of Nup170p. Similarly, a *sir2Δ* mutation did not appear to alter the subtelomeric association of Nup170p (Figure S6). These results are consistent with Sir4p functioning, directly or indirectly, to facilitate Nup170p binding to subtelomeric chromatin.

Nup170p Facilitates Sir4p Binding to Subtelomeric DNA

We hypothesized that the function of Nup170p in subtelomeric gene silencing is linked to its physical association with Sir4p. Because chromatin association of Sir4p is considered a prerequisite for its role in silencing, we examined the effect of Nup170p depletion on the association of Sir4p with its chromatin-binding partner Rap1p. In WT cells, Sir4-9xMyc is detected bound to isolated Rap1-pA, but this interaction was greatly reduced in the absence of Nup170p (Figure 7A). ChIP analysis also revealed that Sir4p binding to DNA regions adjacent to a representative telomere (Tel6R) were reduced ~3-fold in the absence of Nup170p (Figure 7B). Similarly, the Sir4p binding partners Sir2-9xMyc and Sir3-9xMyc also showed reduced association with Tel6R (Figure S6), consistent with the established role of Sir4p in facilitating Sir2p and Sir3p binding to subtelomeric chromatin (reviewed in Rusche et al., 2003). These observations were in sharp contrast to results for Rap1p, which showed enhanced binding to Tel6R and its subtelomeric regions in the absence of Nup170p (Figure S6). Although the basis for the increased binding of Rap1p is unclear, this phenotype further supports the conclusion that Nup170p plays a physiological role at telomeres.

The role of Nup170p in Sir4p localization was also examined by fluorescence microscopy. Sir4p is generally detected in six to eight telomere clusters positioned along the nuclear periphery (Gotta et al., 1996). Mutations that reduce Sir4p binding to telomeres impair clustering, and Sir4p foci redistribute to the nuclear interior (Cockell et al., 1995). We observed 67% of Sir4-GFP foci at the NE in WT and *nup157Δ* cells (Figure 7C). However, cells lacking Nup170p exhibited a diffuse intranuclear Sir4-GFP signal and the peripheral localization of Sir4-GFP foci was reduced to

Figure 2. Nup170p Binds the RSC Complex

(A) The Nup170-pA fusion was affinity purified from cells producing the indicated GFP fusion proteins. Bound complexes were released by stepwise elution using increasing concentrations of $MgCl_2$ (Mg^{2+}) and a final acetic acid wash (AA). Eluted proteins were analyzed by SDS-PAGE and western blotting to detect the indicated proteins. Samples of the total cell lysates (load) and the final wash (wash) prior to elution are shown.

(B–I) Experiments similar to those described in (A) were performed using strains that produced the indicated pA- and/or 13xMyc-tagged proteins. Asterisks indicate IgG cross-reacting species in AA fractions.

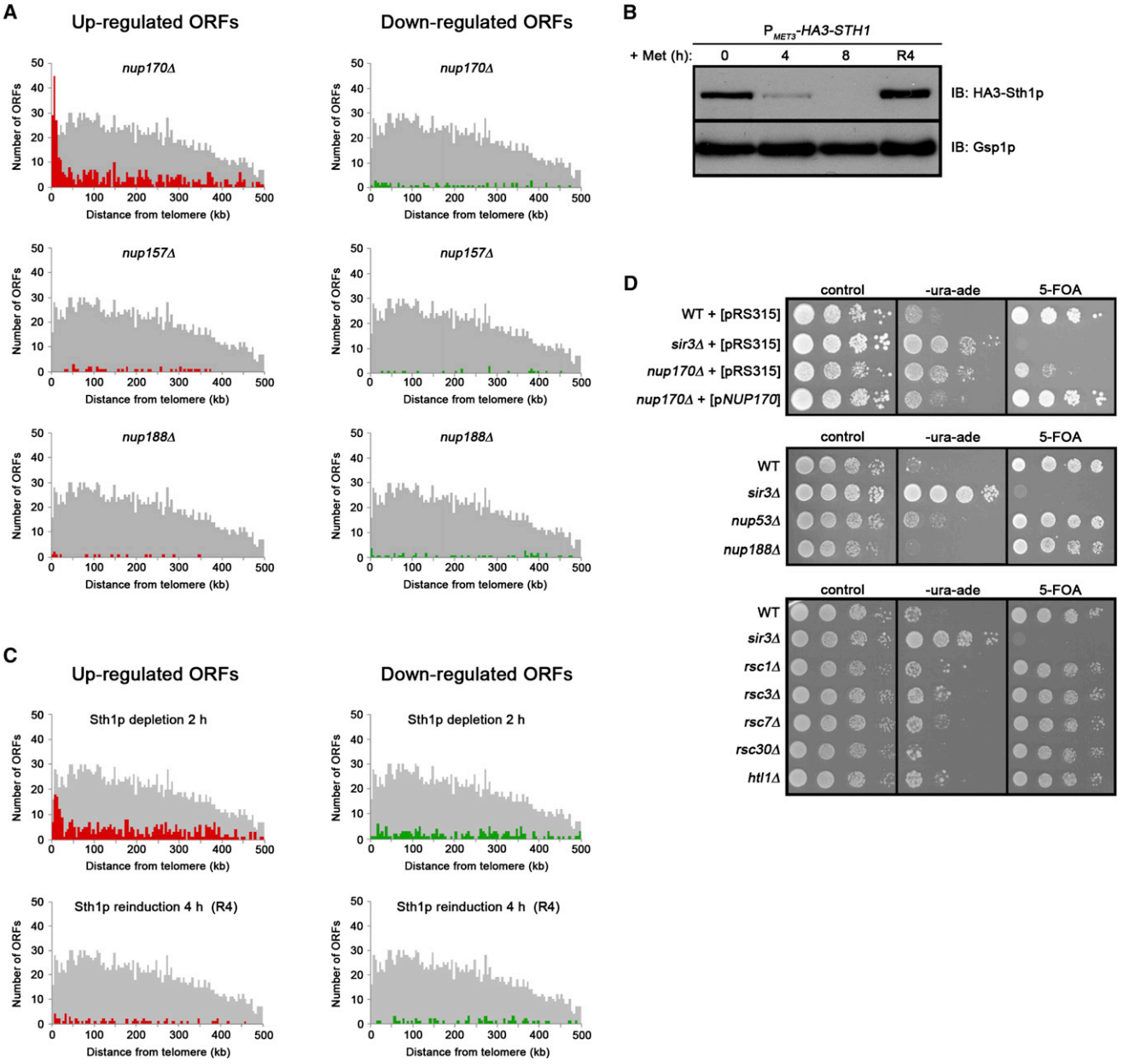

Figure 3. Nup170p Is Required for Subtelomeric Gene Silencing

(A) Gene-expression profiles of *nup170Δ*, *nup157Δ*, and *nup188Δ* cells were determined by DNA microarray analysis. The positions of ORFs identified as differentially expressed (lambda $\geq$ 100) and exhibiting a 2-fold increase (red) or decrease (green) in transcript levels along the length of the chromosomes were determined and the number of altered genes within 5 kb bins (y axis) was plotted versus their distance from chromosome ends (x axis). The distribution of all ORFs within these 5 kb bins is represented in gray; the number of ORFs in each bin is three times that shown on the y axis.

(B and C) Cells containing P_{MET3}-*HA3-STH1* were depleted of Sth1p by addition of methionine for the indicated times. Western blotting (B) was used to detect HA3-Sth1p (IB: HA) and a loading control (IB: Gsp1p).

(C) Microarray analysis was performed on Sth1p-depleted cells (2 hr) and then following reinduction of *STH1* for 4 hr (R4), and data were analyzed as described in (A) except that a λ value $\geq$50 was used.

(D) Silencing of the subtelomeric reporter genes *URA3* and *ADE2* was examined in the indicated haploid strains containing either no plasmid (middle and bottom), empty vector (pRS315), or pHNP170 (p*NUP170*; top). Cell growth was examined under nonselective (control) and selective (lacking uracil and adenine [-ura-ade] or plus 5-FOA [5-FOA]) conditions.

See also Figure S1 and Tables S3 and S4.

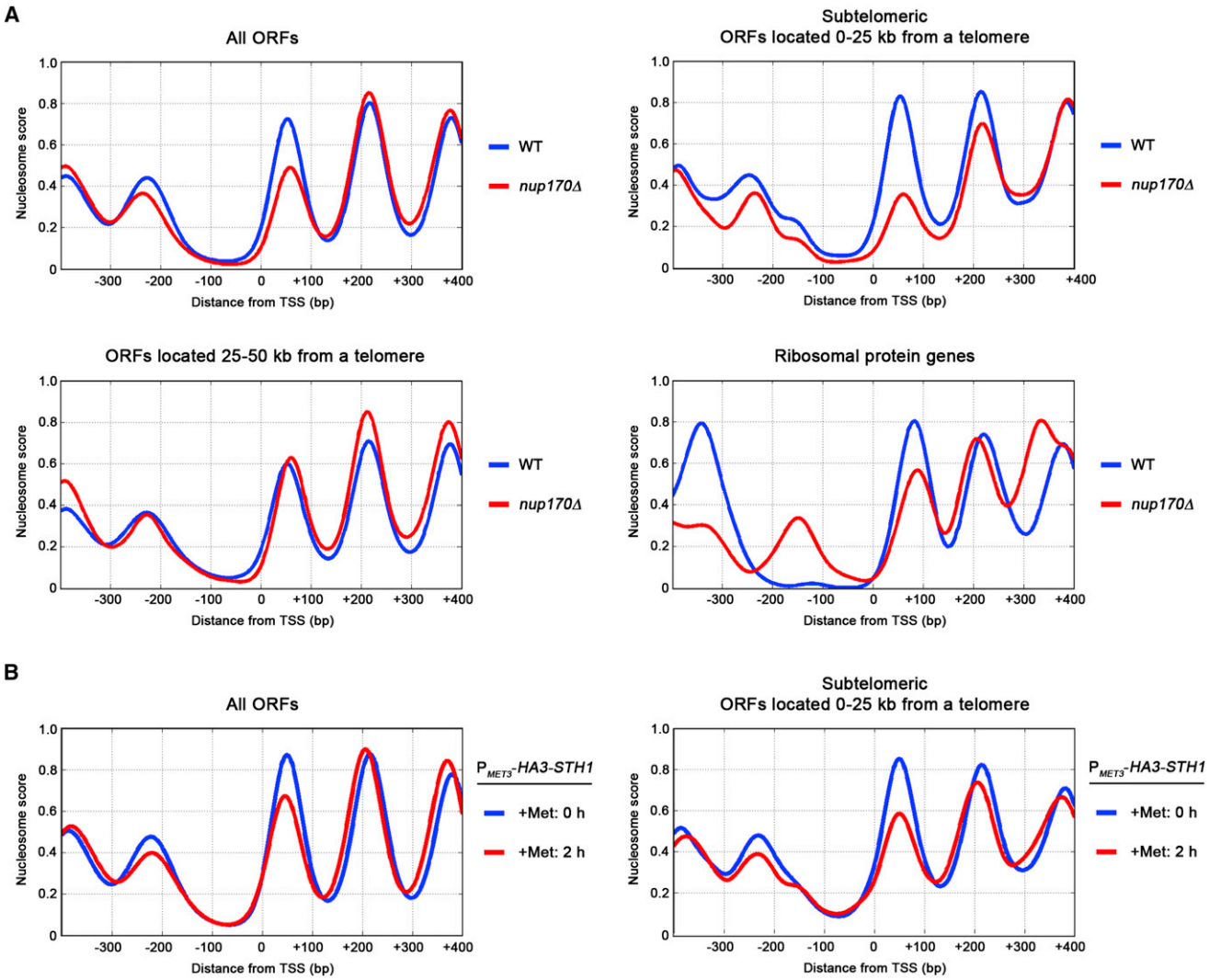

Figure 4. Nup170p Is Required for Nucleosome Positioning

(A) TSS-aligned average nucleosome scores derived from the analysis of WT (blue) and *nup170Δ* (red) cells. Shown is the genome-wide profile (5419 ORFs; top left) and profiles for ORFs located within 0–25 kb (149 ORFs; top right) and 25–50 kb (343 ORFs; bottom left) from chromosome ends. Similar analysis was performed on 138 RP genes (bottom right).

(B) TSS-aligned average nucleosome scores were also obtained from cells depleted of Sth1p for 0 hr (blue) and 2 hr (red). All ORFs (5,419; left) and ORFs located within 0–25 kb regions (right) are shown.

See also Figure S2.

41%, similar to what was observed in the tethering deficient *yku70Δ* mutant (Figure 7C). Importantly, the decreased NE association of Sir4p in the *nup170Δ* mutant did not appear to be due to changes in the localization of its NE receptors Esc1p and Mps3p (Figure S7B), nor did loss of *NUP170* impair the ability of Esc1p to tether a tagged chromosomal locus to the NE (Figure S7C).

Our results support a model in which Nup170p facilitates Sir4p association with subtelomeric chromatin-binding sites, including the telomere-associated protein Rap1p. Unlike Nup170p, the Rap1-interacting factor Rif1p antagonizes Sir4p binding to subtelomeric chromatin by competing with Sir4p for binding to Rap1p (Buck and Shore, 1995). We hypothesized that removing Rif1p and suppressing its antagonistic function would compensate for the loss of Nup170p and restore subtelomeric association of Sir4p. In support of this idea, the introduction of a *rif1Δ* mutation into a *nup170* null mutant (*nup170Δ rif1Δ*) rescued the NE localization of Sir4-GFP to WT levels (Figure 7C). Moreover, deletion of *RIF1* suppressed the silencing defect of the *nup170Δ* mutant, further linking the loss of the silencing phenotype of *nup170Δ* cells to compromised Sir4p function (Figure S1).

Telomere Tethering to the NE Requires Nup170p

Because Sir4p supports telomere tethering to the NE, we examined whether Nup170p also plays a role in telomere positioning.

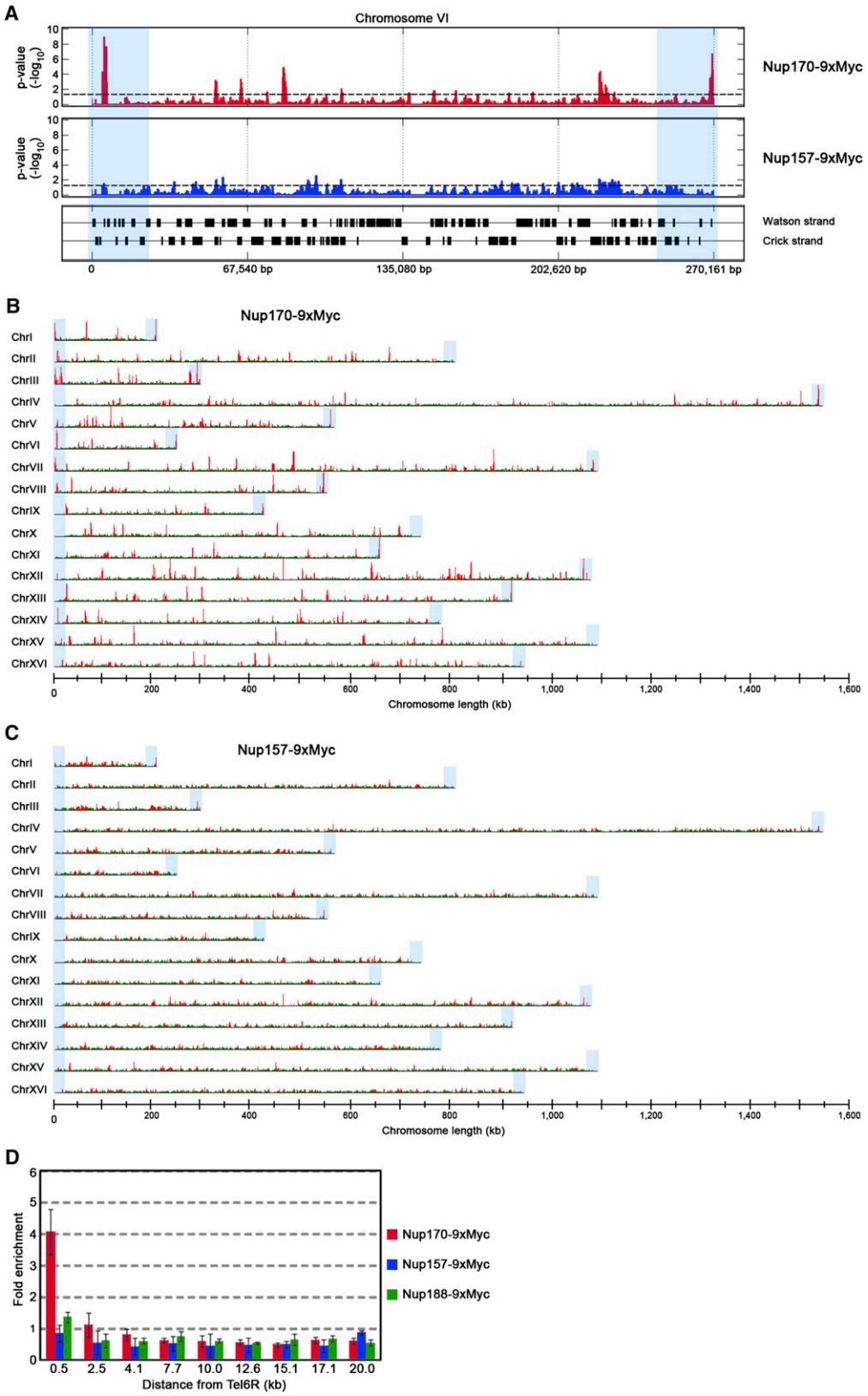

(legend on next page)

We tagged several commonly studied telomeres, Tel6R, Tel8L, and Tel14L, with 256 *lac* operators (*lacO*) in cells producing the *lacO*-binding protein GFP-LacI (Hediger et al., 2002b). We then examined the telomere position relative to the NE marker Sec63-GFP, and scored the foci for their localization within three concentric zones of equal area (Figures 7D and S7; Table S5). As was previously observed (Hediger et al., 2002b), in WT cells Tel6R, Tel8L, and Tel14L were detected in zone 1 immediately underlying the NE (~70% of foci) during G1 and S phases. Similar results were obtained in *nup2Δ* or *nup157Δ* mutants (Figures 7D and S7; Table S5). However, the NE association of all three telomeres was compromised in *nup170Δ* cells during G1 phase, similar to what was detected in *yku70Δ* and *sir4Δ* mutants (also see Hediger et al., 2002b; Hiraga et al., 2008). In contrast to *sir4Δ* mutants, *nup170Δ* cells showed no defects in telomere localization in S phase cells. Consistent with the effect of Nup170p loss on these individual telomeres, Rap1 foci (representative of telomere clusters) showed a similar G1-phase-specific decrease in NE association in the *nup170Δ* cells (Figure 7E). Thus, we conclude that Nup170p plays an essential role in the localization of telomeres during G1 phase of the cell cycle.

DISCUSSION

The INM in most cell types interacts with condensed and/or silenced chromatin. By contrast, studies in yeast and metazoan cells have established functional links between specific Nups and transcriptionally active genes. Thus, the interfaces between NPCs and the INM are likely transitional zones between chromatin states. We have uncovered functional interactions between Nup170p and chromatin domains that generally reside adjacent to the NE, including subtelomeric and telomeric regions. We propose that Nup170p establishes a platform at the NPC that interacts with these chromatin regions and promotes transcriptional repression of RP genes and subtelomeric chromatin. In the context of subtelomeric chromatin, Nup170p functionally interacts with RSC and Sir4p, facilitating Sir4p assembly on subtelomeric heterochromatin, chromatin association with the NE, and repression of resident gene expression.

The functional links between Nup170p and various chromatin-modifying factors suggest that Nup170p contributes to a function that is distinct from but related to that of its genetically interacting partners, including transcriptional repression and heterochromatin assembly. Set3C and Rpd3L are histone deacetylases (HDACs) with roles in silencing (Ehrentraut et al., 2010), and Bre1p and its interactors mediate silencing through their downstream effects on histone H3 methylation (Sun and Allis, 2002). SWR1 also contributes to silencing by defining heterochromatin regions through exchange of canonical histone H2A for the histone variant H2A.Z (Htz1p), notably near telomeres (Mizuguchi et al., 2004). The specific genetic interactions discovered for *NUP170*, as well as other data presented here, lead us to conclude that Nup170p contributes to chromatin structure, including heterochromatin formation and subsequent gene silencing, through parallel activities with its genetically interacting complexes.

This concept is supported by results documenting a role for Nup170p in the organization of nucleosomes in vivo (Figure 4), evidence that a Nup functions in this capacity. Analysis of the *nup170Δ* mutant revealed a decrease in −1 and +1 nucleosome occupancy. These changes were nonrandom and most prominent in subtelomeric chromatin and at RP genes. Although the mechanistic role of Nup170p in nucleosome positioning is unclear, its physical interaction with Sth1p implies a functional link to RSC. Consistently, loss of RSC activity also leads to aberrant −1 and +1 nucleosome profiles (Badis et al., 2008; Hartley and Madhani, 2009; Figure 4). Moreover, many of the subtelomeric genes showing altered nucleosome structure in Sth1p-depleted cells are also altered in the *nup170Δ* mutant.

Nup170p-associated RSC is also envisaged to contribute to transcriptional repression and the maintenance of subtelomeric and telomeric chromatin. Several observations support this idea. In addition to its role in promoting transcription, RSC also plays a role in transcriptional repression (Angus-Hill et al., 2001; Badis et al., 2008). Notably, loss of Rsc30p function leads to upregulation of RP genes (Angus-Hill et al., 2001), in striking similarity to the loss of Nup170p (Figure S4). Moreover, RSC components are required for normal telomere length (Rsc2p, Rsc4p, Rsc14p, and Htl1p; Askree et al., 2004) and Rap1 localization (Rsc1p and Rsc2p; Hiraga et al., 2008), and depletion of Sth1p derepresses multiple subtelomeric genes and alters Nup170p interactions with subtelomeric chromatin (Figure 3; data not shown). These various functions of RSC underscore what are likely context-dependent roles defined by its subunits and accessory binding factors such as Nup170p. For example, Nup170p could influence RSC function by altering its activity and/or by positioning RSC at defined locations, both at specific chromatin sites and at the NPC.

Numerous observations point to interconnected pathways functioning to control ribosome biogenesis and telomere maintenance, including the identification of shared factors such as Rap1p, which functions in RP gene expression and subtelomeric

Figure 5. Nup170p Is Enriched at Subtelomeric DNA

(A) Binding profiles, as determined by ChIP-chip analysis, of Nup170-9xMyc (red) and Nup157-9xMyc (blue) along chromosome VI are plotted as a logarithmic function of their p values. Black rectangles represent ORFs.

(B and C) Complete genome-wide DNA-binding profiles of Nup170-9xMyc and Nup157-9xMyc. Red peaks mark statistically significant binding sites with $p \leq 0.05$, and green peaks mark statistically insignificant binding sites. Peak height is inversely proportional to p value (y axis; $-\log_{10}$, scale = 10). In (A)–(C) subtelomeric regions are highlighted by blue shading. Note that too few probes were available on chips to accurately evaluate significant binding to six subtelomeric regions (0–10 kb): Tel9L, Tel10L, Tel10R, Tel16L (zero probes); Tel15R (one probe); and Tel4L (two probes).

(D) ChIP of Nup170-9xMyc (red), Nup157-9xMyc (blue), and Nup188-9xMyc (green) followed by qPCR using primer sets positioned along a 20 kb subtelomeric region of the right arm of chromosome VI (x axis). Mean relative enrichment of three independent ChIP experiments is plotted on the y axis. Error bars express SE. See also Figures S3, S4, and Tables S3 and S4.

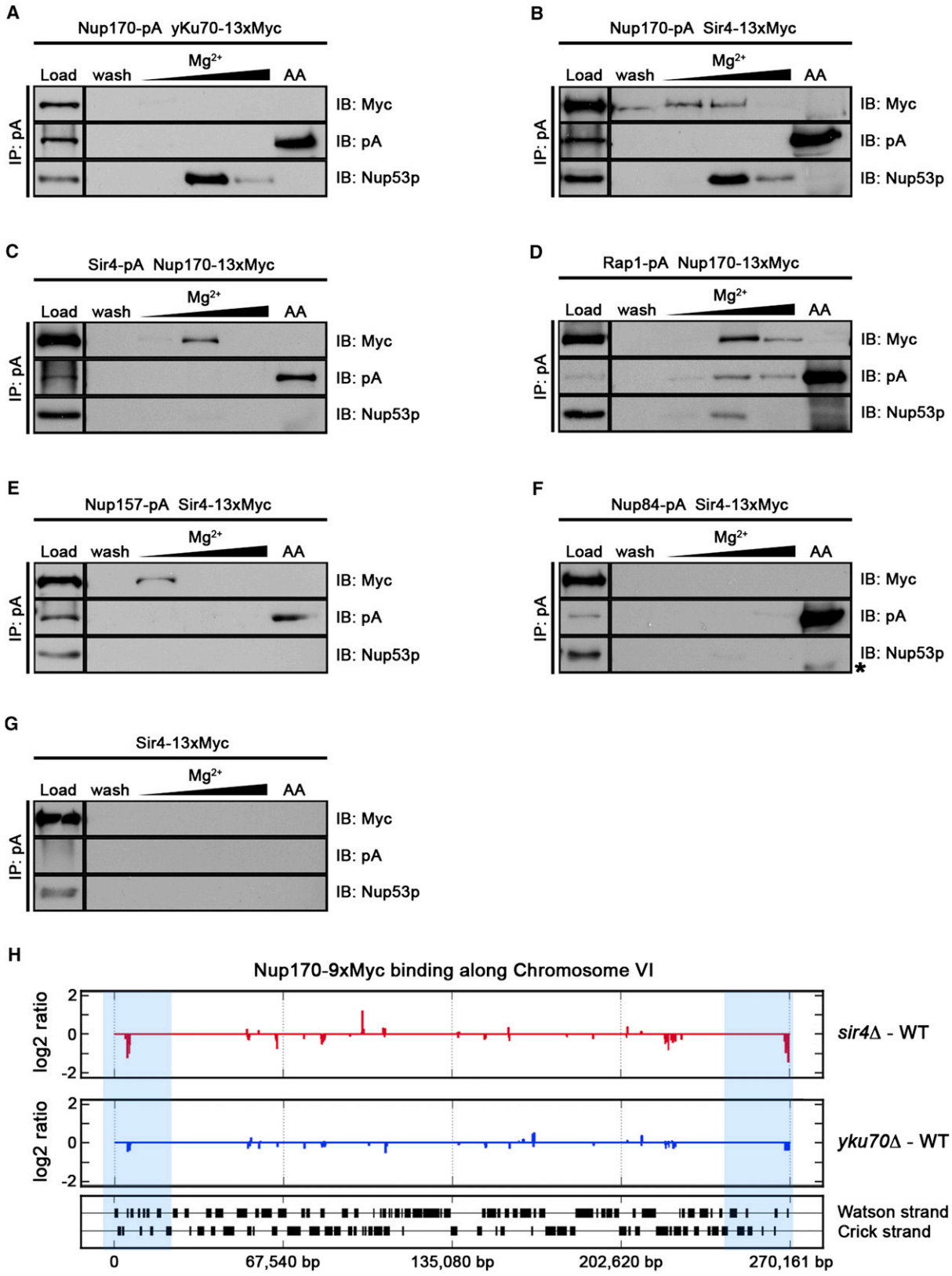

(legend on next page)

gene silencing (Bosio et al., 2011). Our results place Nup170p in a similar regulatory network. Nup170p interacts with virtually all RP genes (131 of 138 meet statistical cutoffs; Figure S4), potentially through its interaction with Rap1p (Figure 6), and represses their expression. This is in contrast to previous studies that concluded that NPC association of RP genes was a consequence of the transcriptional "on" state of these genes (Casolari et al., 2004; Yoshida et al., 2010); however, whether this interaction promotes RP gene expression was not investigated. Interestingly, the localization of one NE-associated RP gene that showed increased expression in the absence of Nup170p, *RPL9A*, was not altered in the *nup170Δ* mutant (Figure S4C). This result implies that increased *RPL9A* expression arose not from a change in the gene's association with the NE, but rather from the loss of a Nup170p-mediated repressive function. We infer that binding sites for activated genes at the NPC are distinct from chromatin-binding regions established by Nup170p and its associated repressive activities.

We also detected physical interactions between Nup170p and subtelomeric regions of one or both ends of all chromosomes analyzed (Figure 5). The idea that NPCs interact with telomeres was previously suggested but has been controversial, as data supporting this claim were indirect. Mlp2p was suggested to anchor telomeres to NPCs (Galy et al., 2000; Feuerbach et al., 2002), but other investigators did not detect such activity (Hediger et al., 2002a, 2002b). More recently, mutations in Nup84 complex members were shown to alter the NE association of Tel11L and Sir3p, and suppress subtelomeric silencing (Therizols et al., 2006). However, the mechanistic link between the Nup84 complex and telomeres is unclear, and the interpretation of these observations is confounded by pleiotropic effects of mutations in the Nup84 complex on NPC structure and function. By comparison, loss of Nup170p does not appear to alter NE structure or active transport (Aitchison et al., 1995; Shulga et al., 2000; Makio et al., 2009).

Our analysis of Nup170p also provides a molecular basis for its contribution to subtelomeric gene silencing. We show that Nup170p physically and functionally interacts with Sir4p and Rap1p (Figure 6), and our data support a model in which the interaction of Nup170p with Sir4p promotes their binding to subtelomeric chromatin (Figures 6, 7, and S5). For example, most subtelomeric binding sites for Nup170p (at least 19 of 23) show dramatic sensitivity to the loss of Sir4p. Similarly, Nup170p is required for the association of Sir4p with Rap1p and the NE, as well as Sir4p binding to a representative telomere, Tel6R (Figure 7). Consistent with the latter observation, in *nup170Δ* cells most Sir4p is intranuclear, whereas telomeres are NE bound during S phase.

The interactions of Nup170p with Sir4p and telomeres are likely regulated and may occur during distinct molecular events such as Sir4p assembly on telomeres. This conclusion is based in part on observations that telomeres exhibit limited colocalization with NPCs when asynchronous cell populations are examined by fluorescence microscopy (Taddei et al., 2004, and data not shown). This lower frequency of colocalization is perhaps not surprising when one considers that telomere association with the NE is transient, with resident times ranging from seconds to several minutes (Hediger et al., 2002b; Hiraga et al., 2006; Ebrahimi and Donaldson, 2008). This is interpreted to reflect the dynamic nature of telomere binding to NE tethering factors, such as Esc1p and Mps3p, and may explain the observations that the bulk of Esc1p fails to colocalize with Sir4p and telomeres (Taddei et al., 2004), and that Mps3p is present predominantly at spindle pole bodies (Jaspersen et al., 2002).

Built upon the dynamic nature of telomere interactions with the NE are cell-cycle-specific mechanisms that mediate these interactions. Although they are chiefly NE associated in interphase, during the later stages of DNA replication telomeres and Sir4p are dispersed throughout the nucleoplasm until the later stages of mitosis, when they again relocalize to the NE (Laroche et al., 2000; Ebrahimi and Donaldson, 2008). During interphase, Sir4p and the yKu70/yKu80 heterodimer play distinct roles in telomere binding to the NE (reviewed in Taddei et al., 2010). For example, yKu70 is required for NE anchoring of Tel14L only during G1 phase, whereas loss of Sir4p disrupts Tel14L localization during G1 and S phases (Hediger et al., 2002b; Figures 7 and S7). We also detect a role for Nup170p in telomere localization to the NE that appears to be linked to the cell cycle, with the loss of Nup170p reducing telomere association with the NE during G1 phase (Figure 7). Moreover, we observed that the interactions of Nup170p with Sir4p are most robust in M-phase-arrested cells (Figure S7D). These results suggest that Nup170p may function primarily in mitosis or during G1 phase to position telomeres at the NE. Importantly, the timing of these interactions approximately coincide with mitotic events that have been proposed to establish subtelomeric gene silencing (see Young and Kirchmaier, 2012). This would explain the loss of subtelomeric silencing observed in *nup170Δ* cells despite the ability of telomeres to reassociate with the NE during S phase.

The interactions of Nup170p with Rap1p, Sir4p, and the RSC complex provide molecular insight into the composition of what is likely one of several chromatin-binding platforms at the NPC. We envisage Nup170p positioned adjacent to the pore membrane (Alber et al., 2007; Makio et al., 2009) with domains extending into the nucleoplasm. However, a clear picture of

Figure 6. Nup170p Association with Subtelomeric DNA Is Mediated by Sir4p

(A–G) Protein-A-tagged chimeras were affinity purified from lysates containing the indicated 13xMyc-tagged proteins as described in Figure 2. The asterisk indicates an IgG cross-reacting band.

(H) Genome-wide binding profiles of Nup170-9xMyc in WT, *sir4Δ*, and *yku70Δ* cells were determined by ChIP-chip, and the binding profiles from WT cells were compared with those from *sir4Δ* (red) and *yku70Δ* (blue) along chromosome VI (x axis). Plotted is the fold enrichment of DNA associated with Nup170-9xMyc isolated from mutant cells minus that from WT cells where $p \leq 0.05$ (y axis; $-\log_2$). Values plotted below the red or blue horizontal line indicate the degree of decreased binding in the mutant strain. Subtelomeric regions are indicated by blue shading.

See also Figures S5, S6, and S7.

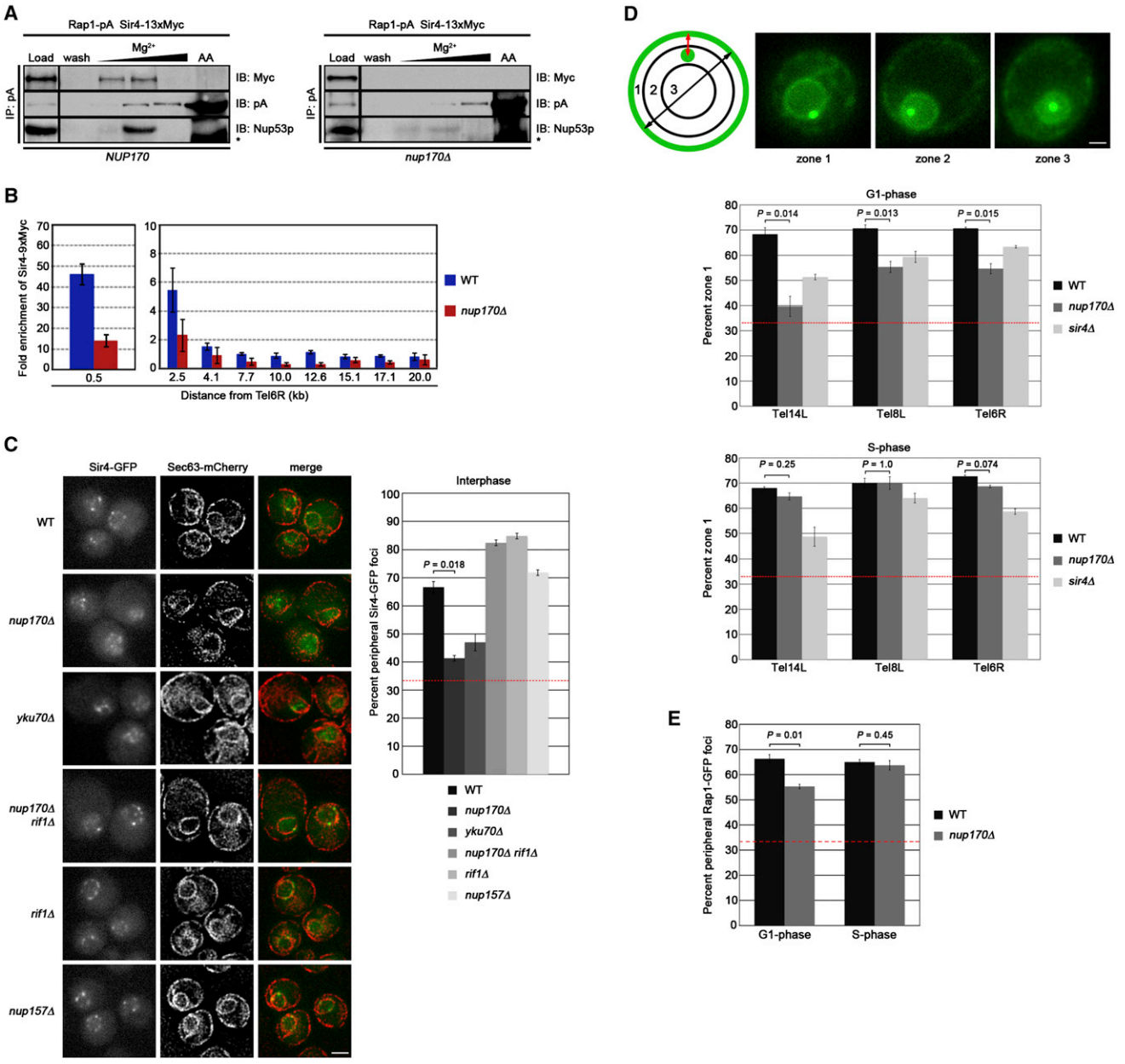

Figure 7. Nup170p Facilitates Sir4p Binding to Subtelomeric DNA

(A) Rap1-pA was affinity purified from cells producing Sir4-13xMyc and containing (*NUP170*) or lacking (*nup170Δ*) Nup170p (right), and analyzed as in Figure 2. Asterisks indicate IgG cross-reacting bands.

(B) ChIP of Sir4-9xMyc followed by qPCR was performed on samples from WT and *nup170Δ* strains as described in Figure 5. Error bars express SE.

(C) The indicated strains expressing *SIR4-GFP* and *SEC63-mCherry* were analyzed by fluorescence microscopy. A deconvolved Sec63-mCherry signal was used to demarcate the NE. Histograms show the percentage of Sir4-GFP foci (based on >400 foci counted per strain) localized at the NE in interphase cells. Mean percentage and SE are shown (n = 3). Scale bar: 2 μm.

(D) Telomere positioning was analyzed in asynchronous cultures of WT, *nup170Δ*, and *sir4Δ* cells. Tel6R, Tel8L, and Tel14L were visualized using integrated *lacO* repeats and GFP-LacI. The subnuclear position of GFP foci in a single focal plane was determined relative to the NE marker Sec63-GFP and assigned to one of three concentric nucleoplasmic zones of equal area (see schematic and representative single focal plane images). The subnuclear positions of 100 foci for Tel14L and 50 foci for Tel6R and Tel8L were determined in unbudded (G1 phase) and small budded (S phase) cells. The mean percentages of telomere foci localized in zone 1 are shown; error bars express SE (n = 3). Scale bar: 1 μm.

(E) The percentage of Rap1-GFP foci localized at the NE in G1 and S phases was determined in WT and *nup170Δ* cells. For each experiment, >200 foci were counted per strain. The mean percentage and SE of three independent experiments are shown. In (C)–(E), random distributions are indicated by the red dashed line at 33%, and the statistical significance of the difference between *nup170Δ* and WT cells is indicated (Student's t test).

See also Figures S6, S7, and Table S5.

this molecular interface awaits a higher-resolution structure for what is likely a very dynamic and flexible NPC. Although Nup170p contributes to gene silencing and heterochromatin structure, other Nup platforms are predicted to interface with activated genes to augment transcription and mRNA export, and to facilitate transcriptional memory (reviewed in Taddei et al., 2010; Van de Vosse et al., 2011). Still other Nups may function in establishing boundaries between silenced and transcriptionally active chromatin (Ishii et al., 2002; Dilworth et al., 2005) or assist in DNA double-strand break repair (Therizols et al., 2006). Our analysis of Nup170p highlights the ability of NPCs to bind and potentially regulate chromatin modifiers (e.g., RSC) that in turn define local chromatin structure. Although we concentrated on these functions in this work, a less clear function is the potential role played by chromatin and chromatin modifiers in NPC structure and assembly. For example, recent evidence suggests that RSC contributes to the structural organization of the NPC (Titus et al., 2010), and we have detected similar functions for other chromatin modifiers (data not shown).

The molecular interactions between the yeast Nup170p-containing complex and Sir4p, as well as the interactions of Sir4p with Mps3p, may be conserved at the interface between NPCs and heterochromatin in higher eukaryotes. Intriguingly, Sun1, a mammalian protein that shares homology with Mps3p, localizes to the INM and NPCs (Liu et al., 2007), where it interacts with heterochromatin and, in cells undergoing meiotic division, contributes to telomere tethering at the NE (Ding et al., 2007). At the NPC, Sun1 appears to interact with Pom121 (Talamas and Hetzer, 2011), which would place Sun1 in close proximity to another binding partner of Pom121, Nup155 (the mammalian counterpart of Nup170p; Mitchell et al., 2010). Strikingly, Sun1, Nup155, and Nup53 all interact with nuclear lamins, and these Nups have been proposed to sit at the interface between the NPC and the nuclear lamina (Hawryluk-Gara et al., 2005; Crisp et al., 2006; J. Mitchell and R.W.W, unpublished data). When we compare yeast and vertebrate complexes, Sir4p and vertebrate lamins appear to be unrelated. However, these proteins may in fact share similar functions. More than two decades ago, Diffley and Stillman (1989) reported on structural similarities between Sir4p and lamin A/C. Although the similarities between these proteins lie within commonly found coiled-coil motifs, their conserved binding partners, association with the INM, and links to silencing suggest that Sir4p and the lamins share at least a subset of functional properties. We also speculate that similarly to Nup170p, Nup155 functions as a chromatin-binding platform, an idea that is consistent with a reported interaction between Nup155 and the histone deacetylase HDAC4 (Kehat et al., 2011).

EXPERIMENTAL PROCEDURES

A detailed description of the methods employed in this study is provided in the Extended Experimental Procedures.

Yeast Strains

The yeast strains used in this study are listed in Table S6.

SGA

SGA analyses were performed as previously described (Tong et al., 2001) except that, to minimize genome instability associated with a *nup170Δ* null mutant (Kerscher et al., 2001), a plasmid-borne WT copy of *NUP170* was maintained throughout the screen until it was removed at the final step of single- and double-mutant selection by addition of 5-FOA.

Affinity Purifications

Yeast cells expressing protein-A-tagged fusion proteins were frozen in liquid nitrogen and lysed using a planetary ball mill (Retsch). Affinity purification of pA fusion proteins from cell lysates was performed using immunoglobulin G (IgG)-coupled magnetic beads.

Gene Expression Profiling

Two-color microarrays were performed using whole-genome *S. cerevisiae* arrays (Agilent). All experiments were performed with duplicate experimental and technical replicates of each condition as previously described (Wan et al., 2009).

Subtelomeric Silencing Assay

Ten-fold serial dilutions of cell cultures were spotted onto one of three sets of plates: (1) synthetic complete (SC) medium, SC-ura-ade, and SC + 1 mg/ml 5-FOA; (2) SC-leu, SC-leu-ura-ade, and SC-leu + 1 mg/ml 5-FOA; or (3) YPD medium. Plates were incubated for 2–5 days at 30°C and then kept at 4°C for an additional 10 days to permit color development.

Genome-wide Nucleosome Positioning Analysis

Mononucleosomal DNA was isolated as previously described (Yuan et al., 2005) and subjected to Illumina sequencing.

ChIP

ChIP was performed as described by Wan et al. (2009). Real-time qPCR was performed as previously described (Wan et al., 2009). Genome-wide chromatin localization analysis (ChIP-chip) was performed using Agilent whole-genome *S. cerevisiae* arrays and processed with Agilent Feature Extraction and Agilent ChIP Analytics software.

Fluorescence Microscopy

Yeast strains producing GFP-tagged and/or mCherry-tagged fusion proteins were immobilized on 2% agarose pads containing SC medium. Images were acquired as a series of 14 section z stacks and processed using ImageJ software (National Institutes of Health). Analysis of the subnuclear positioning of Sir4-GFP and Rap1-GFP foci was aided by iterative deconvolution of the Sec63-mCherry signal to enhance visualization of the NE. Subnuclear positioning of 256 × *lacO*-tagged telomeres was determined as previously described (Hediger et al., 2002b).

ACCESSION NUMBERS

Data from DNA microarray analysis, ChIP-chip analysis, and nucleosome positioning analysis have been submitted to the Gene Expression Omnibus database under accession number GSE36795.

SUPPLEMENTAL INFORMATION

Supplemental Information includes Extended Experimental Procedures, seven figures, and six tables and can be found with this article online at http://dx.doi.org/10.1016/j.cell.2013.01.049.

ACKNOWLEDGMENTS

We thank S.M. Gasser, D.E. Gottschling, C. Boone, S.L. Jaspersen, R. Rachubinski, and B.R. Cairns for providing reagents. We thank T. Makio for construction of the TMY1452 and TMY1798 strains, and Y. Sydorskyy and N. Arens for technical assistance. We also thank E. Hurt, L. Cairo, N. Adames, S. Danziger, and members of the Wozniak and Aitchison laboratories for thoughtful discussions. We thank Allison Kudla for the graphical abstract. Funds for this work were provided to R.W.W. by the CIHR (MOP 36519 MOP 106502), AIHS, and HHMI, and to J.D.A. by the NIH (P50 GM076547 and U54 GM103511).

D.W.V.d.V. was supported by a CIHR Canada Graduate Doctoral Scholarship, and Y.W. was supported by the National Natural Science Foundation of China (31071146 and 31271365).

Received: March 27, 2012
Revised: August 13, 2012
Accepted: January 28, 2013
Published: February 28, 2013

REFERENCES

Aitchison, J.D., and Rout, M.P. (2012). The yeast nuclear pore complex and transport through it. Genetics *190*, 855–883.

Aitchison, J.D., Rout, M.P., Marelli, M., Blobel, G., and Wozniak, R.W. (1995). Two novel related yeast nucleoporins Nup170p and Nup157p: complementation with the vertebrate homologue Nup155p and functional interactions with the yeast nuclear pore-membrane protein Pom152p. J. Cell Biol. *131*, 1133–1148.

Alber, F., Dokudovskaya, S., Veenhoff, L.M., Zhang, W., Kipper, J., Devos, D., Suprapto, A., Karni-Schmidt, O., Williams, R., Chait, B.T., et al. (2007). The molecular architecture of the nuclear pore complex. Nature *450*, 695–701.

Amlacher, S., Sarges, P., Flemming, D., van Noort, V., Kunze, R., Devos, D.P., Arumugam, M., Bork, P., and Hurt, E. (2011). Insight into structure and assembly of the nuclear pore complex by utilizing the genome of a eukaryotic thermophile. Cell *146*, 277–289.

Andrulis, E.D., Neiman, A.M., Zappulla, D.C., and Sternglanz, R. (1998). Perinuclear localization of chromatin facilitates transcriptional silencing. Nature *394*, 592–595.

Angus-Hill, M.L., Schlichter, A., Roberts, D., Erdjument-Bromage, H., Tempst, P., and Cairns, B.R. (2001). A Rsc3/Rsc30 zinc cluster dimer reveals novel roles for the chromatin remodeler RSC in gene expression and cell cycle control. Mol. Cell *7*, 741–751.

Askree, S.H., Yehuda, T., Smolikov, S., Gurevich, R., Hawk, J., Coker, C., Krauskopf, A., Kupiec, M., and McEachern, M.J. (2004). A genome-wide screen for Saccharomyces cerevisiae deletion mutants that affect telomere length. Proc. Natl. Acad. Sci. USA *101*, 8658–8663.

Badis, G., Chan, E.T., van Bakel, H., Pena-Castillo, L., Tillo, D., Tsui, K., Carlson, C.D., Gossett, A.J., Hasinoff, M.J., Warren, C.L., et al. (2008). A library of yeast transcription factor motifs reveals a widespread function for Rsc3 in targeting nucleosome exclusion at promoters. Mol. Cell *32*, 878–887.

Bosio, M.C., Negri, R., and Dieci, G. (2011). Promoter architectures in the yeast ribosomal expression program. Transcription *2*, 71–77.

Buck, S.W., and Shore, D. (1995). Action of a RAP1 carboxy-terminal silencing domain reveals an underlying competition between HMR and telomeres in yeast. Genes Dev. *9*, 370–384.

Casolari, J.M., Brown, C.R., Komili, S., West, J., Hieronymus, H., and Silver, P.A. (2004). Genome-wide localization of the nuclear transport machinery couples transcriptional status and nuclear organization. Cell *117*, 427–439.

Cockell, M., Palladino, F., Laroche, T., Kyrion, G., Liu, C., Lustig, A.J., and Gasser, S.M. (1995). The carboxy termini of Sir4 and Rap1 affect Sir3 localization: evidence for a multicomponent complex required for yeast telomeric silencing. J. Cell Biol. *129*, 909–924.

Crisp, M., Liu, Q., Roux, K., Rattner, J.B., Shanahan, C., Burke, B., Stahl, P.D., and Hodzic, D. (2006). Coupling of the nucleus and cytoplasm: role of the LINC complex. J. Cell Biol. *172*, 41–53.

Diffley, J.F., and Stillman, B. (1989). Transcriptional silencing and lamins. Nature *342*, 24.

Dilworth, D.J., Tackett, A.J., Rogers, R.S., Yi, E.C., Christmas, R.H., Smith, J.J., Siegel, A.F., Chait, B.T., Wozniak, R.W., and Aitchison, J.D. (2005). The mobile nucleoporin Nup2p and chromatin-bound Prp20p function in endogenous NPC-mediated transcriptional control. J. Cell Biol. *171*, 955–965.

Ding, X., Xu, R., Yu, J., Xu, T., Zhuang, Y., and Han, M. (2007). SUN1 is required for telomere attachment to nuclear envelope and gametogenesis in mice. Dev. Cell *12*, 863–872.

Ebrahimi, H., and Donaldson, A.D. (2008). Release of yeast telomeres from the nuclear periphery is triggered by replication and maintained by suppression of Ku-mediated anchoring. Genes Dev. *22*, 3363–3374.

Ehrentraut, S., Weber, J.M., Dybowski, J.N., Hoffmann, D., and Ehrenhofer-Murray, A.E. (2010). Rpd3-dependent boundary formation at telomeres by removal of Sir2 substrate. Proc. Natl. Acad. Sci. USA *107*, 5522–5527.

Feuerbach, F., Galy, V., Trelles-Sticken, E., Fromont-Racine, M., Jacquier, A., Gilson, E., Olivo-Marin, J.C., Scherthan, H., and Nehrbass, U. (2002). Nuclear architecture and spatial positioning help establish transcriptional states of telomeres in yeast. Nat. Cell Biol. *4*, 214–221.

Galy, V., Olivo-Marin, J.C., Scherthan, H., Doye, V., Rascalou, N., and Nehrbass, U. (2000). Nuclear pore complexes in the organization of silent telomeric chromatin. Nature *403*, 108–112.

Gasser, S.M., Hediger, F., Taddei, A., Neumann, F.R., and Gartenberg, M.R. (2004). The function of telomere clustering in yeast: the circe effect. Cold Spring Harb. Symp. Quant. Biol. *69*, 327–337.

Gotta, M., Laroche, T., Formenton, A., Maillet, L., Scherthan, H., and Gasser, S.M. (1996). The clustering of telomeres and colocalization with Rap1, Sir3, and Sir4 proteins in wild-type Saccharomyces cerevisiae. J. Cell Biol. *134*, 1349–1363.

Hartley, P.D., and Madhani, H.D. (2009). Mechanisms that specify promoter nucleosome location and identity. Cell *137*, 445–458.

Hawryluk-Gara, L.A., Shibuya, E.K., and Wozniak, R.W. (2005). Vertebrate Nup53 interacts with the nuclear lamina and is required for the assembly of a Nup93-containing complex. Mol. Biol. Cell *16*, 2382–2394.

Hediger, F., Dubrana, K., and Gasser, S.M. (2002a). Myosin-like proteins 1 and 2 are not required for silencing or telomere anchoring, but act in the Tel1 pathway of telomere length control. J. Struct. Biol. *140*, 79–91.

Hediger, F., Neumann, F.R., Van Houwe, G., Dubrana, K., and Gasser, S.M. (2002b). Live imaging of telomeres: yKu and Sir proteins define redundant telomere-anchoring pathways in yeast. Curr. Biol. *12*, 2076–2089.

Hiraga, S., Robertson, E.D., and Donaldson, A.D. (2006). The Ctf18 RFC-like complex positions yeast telomeres but does not specify their replication time. EMBO J. *25*, 1505–1514.

Hiraga, S., Botsios, S., and Donaldson, A.D. (2008). Histone H3 lysine 56 acetylation by Rtt109 is crucial for chromosome positioning. J. Cell Biol. *183*, 641–651.

Ishii, K., Arib, G., Lin, C., Van Houwe, G., and Laemmli, U.K. (2002). Chromatin boundaries in budding yeast: the nuclear pore connection. Cell *109*, 551–562.

Jaspersen, S.L., Giddings, T.H., Jr., and Winey, M. (2002). Mps3p is a novel component of the yeast spindle pole body that interacts with the yeast centrin homologue Cdc31p. J. Cell Biol. *159*, 945–956.

Kehat, I., Accornero, F., Aronow, B.J., and Molkentin, J.D. (2011). Modulation of chromatin position and gene expression by HDAC4 interaction with nucleoporins. J. Cell Biol. *193*, 21–29.

Kerscher, O., Hieter, P., Winey, M., and Basrai, M.A. (2001). Novel role for a Saccharomyces cerevisiae nucleoporin, Nup170p, in chromosome segregation. Genetics *157*, 1543–1553.

Laroche, T., Martin, S.G., Tsai-Pflugfelder, M., and Gasser, S.M. (2000). The dynamics of yeast telomeres and silencing proteins through the cell cycle. J. Struct. Biol. *129*, 159–174.

Liu, Q., Pante, N., Misteli, T., Elsagga, M., Crisp, M., Hodzic, D., Burke, B., and Roux, K.J. (2007). Functional association of Sun1 with nuclear pore complexes. J. Cell Biol. *178*, 785–798.

Lusk, C.P., Makhnevych, T., Marelli, M., Aitchison, J.D., and Wozniak, R.W. (2002). Karyopherins in nuclear pore biogenesis: a role for Kap121p in the assembly of Nup53p into nuclear pore complexes. J. Cell Biol. *159*, 267–278.

Makio, T., Stanton, L.H., Lin, C.C., Goldfarb, D.S., Weis, K., and Wozniak, R.W. (2009). The nucleoporins Nup170p and Nup157p are essential for nuclear pore complex assembly. J. Cell Biol. *185*, 459–473.

Mendjan, S., Taipale, M., Kind, J., Holz, H., Gebhardt, P., Schelder, M., Vermeulen, M., Buscaino, A., Duncan, K., Mueller, J., et al. (2006). Nuclear

pore components are involved in the transcriptional regulation of dosage compensation in Drosophila. Mol. Cell *21*, 811–823.

Mitchell, J.M., Mansfeld, J., Capitanio, J., Kutay, U., and Wozniak, R.W. (2010). Pom121 links two essential subcomplexes of the nuclear pore complex core to the membrane. J. Cell Biol. *191*, 505–521.

Mizuguchi, G., Shen, X., Landry, J., Wu, W.H., Sen, S., and Wu, C. (2004). ATP-driven exchange of histone H2AZ variant catalyzed by SWR1 chromatin remodeling complex. Science *303*, 343–348.

Ptak, C., Anderson, A.M., Scott, R.J., Van de Vosse, D., Rogers, R.S., Sydorskyy, Y., Aitchison, J.D., and Wozniak, R.W. (2009). A role for the karyopherin Kap123p in microtubule stability. Traffic *10*, 1619–1634.

Rout, M.P., Aitchison, J.D., Suprapto, A., Hjertaas, K., Zhao, Y., and Chait, B.T. (2000). The yeast nuclear pore complex: composition, architecture, and transport mechanism. J. Cell Biol. *148*, 635–651.

Rusche, L.N., Kirchmaier, A.L., and Rine, J. (2003). The establishment, inheritance, and function of silenced chromatin in Saccharomyces cerevisiae. Annu. Rev. Biochem. *72*, 481–516.

Shim, E.Y., Ma, J.L., Oum, J.H., Yanez, Y., and Lee, S.E. (2005). The yeast chromatin remodeler RSC complex facilitates end joining repair of DNA double-strand breaks. Mol. Cell. Biol. *25*, 3934–3944.

Shulga, N., Mosammaparast, N., Wozniak, R., and Goldfarb, D.S. (2000). Yeast nucleoporins involved in passive nuclear envelope permeability. J. Cell Biol. *149*, 1027–1038.

Stark, C., Breitkreutz, B.J., Reguly, T., Boucher, L., Breitkreutz, A., and Tyers, M. (2006). BioGRID: a general repository for interaction datasets. Nucleic Acids Res. *34*(Database issue), D535–D539.

Sun, Z.W., and Allis, C.D. (2002). Ubiquitination of histone H2B regulates H3 methylation and gene silencing in yeast. Nature *418*, 104–108.

Taddei, A., Hediger, F., Neumann, F.R., Bauer, C., and Gasser, S.M. (2004). Separation of silencing from perinuclear anchoring functions in yeast Ku80, Sir4 and Esc1 proteins. EMBO J. *23*, 1301–1312.

Taddei, A., Schober, H., and Gasser, S.M. (2010). The budding yeast nucleus. Cold Spring Harb. Perspect. Biol. *2*, a000612.

Talamas, J.A., and Hetzer, M.W. (2011). POM121 and Sun1 play a role in early steps of interphase NPC assembly. J. Cell Biol. *194*, 27–37.

Therizols, P., Fairhead, C., Cabal, G.G., Genovesio, A., Olivo-Marin, J.C., Dujon, B., and Fabre, E. (2006). Telomere tethering at the nuclear periphery is essential for efficient DNA double strand break repair in subtelomeric region. J. Cell Biol. *172*, 189–199.

Titus, L.C., Dawson, T.R., Rexer, D.J., Ryan, K.J., and Wente, S.R. (2010). Members of the RSC chromatin-remodeling complex are required for maintaining proper nuclear envelope structure and pore complex localization. Mol. Biol. Cell *21*, 1072–1087.

Tong, A.H., Evangelista, M., Parsons, A.B., Xu, H., Bader, G.D., Pagé, N., Robinson, M., Raghibizadeh, S., Hogue, C.W., Bussey, H., et al. (2001). Systematic genetic analysis with ordered arrays of yeast deletion mutants. Science *294*, 2364–2368.

Van de Vosse, D.W., Wan, Y., Wozniak, R.W., and Aitchison, J.D. (2011). Role of the nuclear envelope in genome organization and gene expression. Wiley Interdiscip. Rev. Syst. Biol. Med. *3*, 147–166.

Wan, Y., Saleem, R.A., Ratushny, A.V., Roda, O., Smith, J.J., Lin, C.H., Chiang, J.H., and Aitchison, J.D. (2009). Role of the histone variant H2A.Z/Htz1p in TBP recruitment, chromatin dynamics, and regulated expression of oleate-responsive genes. Mol. Cell. Biol. *29*, 2346–2358.

Weiner, A., Hughes, A., Yassour, M., Rando, O.J., and Friedman, N. (2010). High-resolution nucleosome mapping reveals transcription-dependent promoter packaging. Genome Res. *20*, 90–100.

Yoshida, T., Shimada, K., Oma, Y., Kalck, V., Akimura, K., Taddei, A., Iwahashi, H., Kugou, K., Ohta, K., Gasser, S.M., and Harata, M. (2010). Actin-related protein Arp6 influences H2A.Z-dependent and -independent gene expression and links ribosomal protein genes to nuclear pores. PLoS Genet. *6*, e1000910.

Young, T.J., and Kirchmaier, A.L. (2012). Cell cycle regulation of silent chromatin formation. Biochim. Biophys. Acta *1819*, 303–312.

Yuan, G.C., Liu, Y.J., Dion, M.F., Slack, M.D., Wu, L.F., Altschuler, S.J., and Rando, O.J. (2005). Genome-scale identification of nucleosome positions in S. cerevisiae. Science *309*, 626–630.